Journal of Controlled Release 366 (2024) 548–566

Contents lists available at ScienceDirect

Journal of Controlled Release

journal homepage: www.elsevier.com/locate/jconrel

Intradermal delivery of the antiretroviral drugs cabotegravir and rilpivirine by dissolving microarray patches: Investigation of lymphatic uptake

Inken K. Ramöller [a,1], Fabiana Volpe-Zanutto [a,b], Lalitkumar K. Vora [a], Marco T.A. Abbate [a], Aaron R.J. Hutton [a], Peter E. McKenna [a], Ke Peng [a], Ismaiel A. Tekko [a,c], Akmal Sabri [a], Emma McAlister [a], Helen O. McCarthy [a], Alejandro J. Paredes [a], Ryan F. Donnelly [a,*]

[a] School of Pharmacy, Queen's University Belfast, Medical Biology Centre, 97 Lisburn Road, Belfast BT9 7BL, United Kingdom
[b] Faculty of Pharmaceutical Sciences, R. Cândido Portinari, 200 - Cidade Universitária, University of Campinas, Campinas, SP 13083-871, Brazil
[c] Faculty of Pharmacy, Aleppo University, Syria

ARTICLE INFO

Keywords:
Cabotegravir
Rilpivirine
Lymph-targeted
Intradermal delivery
Antiretroviral
PrEP
HIV
Lymphatic distribution
Nanocrystals

ABSTRACT

The lymphatic system possesses the main viral replication sites in the body following viral infection. Unfortunately, current antiretroviral agents penetrate the lymph nodes insufficiently when administered orally and, therefore, cannot access the lymphatic system sufficiently to interrupt this viral replication. For this reason, novel drug delivery systems aimed at enhancing the lymphatic uptake of antiretroviral drugs are highly desirable. Dissolving polymeric microarray patches (MAPs) may help to target the lymph intradermally. MAPs are intradermal drug delivery systems used to deliver many types of compounds. The present work describes a novel work investigating the lymphatic uptake of two anti-HIV drugs: cabotegravir (CAB) and rilpivirine (RPV) when delivered intradermally using dissolving MAPs containing nanocrystals of both drugs. Maps were formulated using NCs obtained by solvent-free milling technique. The polymers used to prepare the NCs of both drugs were PVA 10 Kda and PVP 58 Kda. Both NCs were submitted to the lyophilization process and reconstituted with deionized water to form the first layer of drug casting. Backing layers were developed for short application times and effective skin deposition. In vivo biodistribution profiles of RPV and CAB after MAP skin application were investigated and compared with the commercial intramuscular injection using rats. After a single application of RPV MAPs, a higher concentration of RPV was delivered to the axillary lymph nodes (AL) (C_{max} 2466 ng/g – T_{max} 3 days) when compared with RPV IM injection (18 ng/g - T_{max} 1 day), while CAB MAPs delivered slightly lower amounts of drug to the AL (5808 ng/g in 3 days) when compared with CAB IM injection (9225 ng/g in 10 days). However, CAB MAPs delivered 7726 ng/g (T_{max} 7 days) to the external lumbar lymph nodes, which was statistically equivalent to IM delivery (C_{max} 8282 ng/g - T_{max} 7 days). This work provides strong evidence that MAPs were able to enhance the delivery of CAB and RPV to the lymphatic system compared to the IM delivery route.

1. Introduction

According to the World Health Organization (WHO), human immunodeficiency virus (HIV) continues to be a major global public health issue, having claimed >32 million lives thus far. Currently, approximately 38 million people are living with HIV, with 1.7 million people contracting new infections each year. Although HIV is a global disease, the most affected region is the African continent. To date, HIV infections are still not curable; however, developments in antiretroviral therapy have helped to control the virus effectively, thus enhancing the quality and outlook of the lives of millions of patients. Accordingly, the number of new HIV infections and HIV-related deaths has fallen considerably over the last 20 years [1]. Highly active antiretroviral therapy (HAART) was introduced widely in 1996 and dramatically increased the life expectancy of HIV-infected individuals [2]. HAART uses a combination of drugs with different therapeutic targets. The aim of HAART is to prevent mortality and morbidity associated with chronic HIV infections while minimizing drug toxicity. The combination of different drugs increases

* Corresponding author at: Pharmaceutical Technology, School of Pharmacy, Queens University Belfast, Medical Biology Centre, 97 Lisburn Road, Belfast BT9 7BL, Northern Ireland, United Kingdom.
E-mail address: r.donnelly@qub.ac.uk (R.F. Donnelly).
[1] These authors contributed equally to this work

https://doi.org/10.1016/j.jconrel.2024.01.010
Received 31 August 2023; Received in revised form 5 January 2024; Accepted 8 January 2024
Available online 13 January 2024

efficiency and reduces the development of drug resistance. According to the guidelines of the WHO, a daily oral regimen is recommended for the treatment of HIV [3]. However, for some user groups, daily treatment via the oral route can be challenging, with instances of poor adherence and, therefore, resistance development and treatment failure commonly reported [4]. Consequently, current research focuses on alternative prevention and treatment strategies involving the application of long-acting antiretrovirals to reduce total pill burden and dosing frequency.

In January 2021, the US Food and Drug Administration (FDA) approved Cabenuva (cabotegravir (CAB) + rilpivirine (RPV) prolonged-release suspension for injection, ViiV Healthcare) [5] for the combined treatment of HIV-1 infections in adults via monthly or bimonthly injections. The potential of this new system is considered by many to be high, as the treatment intervals are greatly reduced compared to daily oral medication. Nevertheless, injections have many drawbacks. In a phase III clinical trial [6], long-acting injectable therapy was compared to oral medication with RPV and CAB. The injectable regimen was favored by 86% of participants as their preferred HIV treatment, showing the great impact of this approach. However, 75% of participants experienced pain at the injection sites. Nodules (12%) and indurations (10%) were also reported [6]. In addition to pain, the deliverability of injectables is resource intensive. In low-resource settings, such as Sub-Saharan Africa, the availability of the adequately trained healthcare staff required for safe and appropriate injection administration is less than that of a high-resource region. Furthermore, the ability of patients in these settings to attend healthcare facilities, which are often situated considerable distances from their homes, to receive treatment is also reduced. Stability issues, particularly during "the last mile" of storage prior to administration, are also a significant barrier to treatment for patients who live in low-resource settings [4]. It is for reasons such as this that an unmet need for effective HIV therapies still exists in areas such as Sub-Saharan Africa and why continued innovation in this field is necessary to make effective HIV therapy more widely available. New methods and delivery systems – designed with users, providers, and other stakeholders in mind – could address constraints that affect the ease of use, acceptability, supply and provision.

Microarray patches (MAPs) are novel transdermal drug delivery systems that could improve both the lymphatic uptake of antiretrovirals and the acceptability and access to HIV treatment. MAPs are minimally invasive devices composed of microneedles (MNs) that are <1 mm in length regularly arranged on a flat baseplate to form a patch that can be easily self-administered to the skin. It is impossible to reinsert dissolving MAPs into the skin following effective application; thus, the risk of infectious disease transmission via needle sharing or needle-stick injury is eliminated [7]. A further advantage regarding lymph-targeted drug delivery is that the interstitial oncotic fluid pressure is higher in the skin than those in other injection sites. This phenomenon is explained because the lymph vessel density in skin is higher than that in muscle or subcutaneous tissue [8]. Therefore, the intradermal application of therapeutic agents via MAPs could possibly enhance lymphatic uptake by increasing the concentration of drugs in the lymph without increasing their plasma concentrations. This would impact positively HIV treatment /prevention, because the lymphatic system possesses HIV-targeted immune cells, and it is one of the main viral replication sites in the body following viral infection [9,10]. However, to date, only a few studies have investigated the use of MAPs for the treatment of HIV, and none of these studies have focused on improved lymphatic uptake [11–16].

Lymph-targeted delivery of antiretroviral agents could greatly transform the treatment outcomes for HIV by reducing or suppressing viral reservoirs within the body. Various techniques have been employed previously for passively or actively accessing the lymphatic system. Passive targeting can be achieved by intradermal application of particulate systems in the low nanometer range (10–100 nm) [12], because particles with size range closer to 100 nm have an easy access to the lymphatic capillaries with the ability to accumulate into the regional lymph nodes [17]. In this work, the possibility of delivering antiretroviral nanocrystals (NCs) intradermally by dissolving polymeric MAPs is investigated. NCs are crystalline nanosized drug particles usually made from poorly water-soluble drugs. Considering that the number of poorly water-soluble drugs is increasing steadily, the importance of producing drug NCs, for example, for enhanced bioavailability, has shifted into focus [18]. Their great advantage is that their payload approaches 100%, as they are formulated from the pure drug with only a bare minimum of stabilizers [19]. When NCs are dispersed in a liquid, the formulations are commonly referred to as nanosuspensions [20], whereas the term NCs is commonly used for solid materials. NCs of the antiretroviral agents RPV and CAB with low diameters for improved passive lymphatic uptake were prepared. These were then incorporated into dissolving MAPs, and their design was rationalized in terms of drug delivery efficiency and ease of application [15,16,21], employing a novel multilayered design. MAP characteristics were assessed in vitro and ex vivo for their suitability for in vivo applications. Aside from a possible, desirable alternative to intramuscular injections of long-acting antiretrovirals, the developed MAPs could also be a way to access HIV reservoirs in the lymphatic system.

2. Materials and methods

2.1. Materials

RPV free-base powder and RPV long-acting nanosuspensions (LA NS) (300 mg/mL) were supplied by Janssen Pharmaceutica, Beerse, Belgium. CAB free acid CAB LA NS (200 mg/mL) were kindly supplied by ViiV Healthcare Ltd., Brentford, UK. Parafilm M™ laboratory film was provided by Bemis Company Inc., Soignies, Belgium. Poly (lactic acid) (PLA) (Ultimaker, Geldermalsen, Netherlands). Poly(vinyl pyrrolidone) (PVP) (MW 58 kDa) was sold under the product brand name PlasdoneTM K-29/32 (Ashland, Kidderminster, UK). HPLC grade acetonitrile, phosphate buffered saline (PBS) tablets, poly (vinyl alcohol) (PVA) (MW 31–50 kDa, 80% hydrolyzed), and PVA (MW) 9–10 kDa were purchased from Sigma–Aldrich, St. Louis, MO, USA. Tegaderm™ and Microfoam™ surgical tape (3 M, Bracknell, UK). Trifluoroacetic acid (TFA), reagent grade, > 99% (Honeywell, Seelze, Germany). Veet® sensitive skin hair removal cream (Reckitt Benckiser Group, Slough, England). Water for injections was 100% (*w/v*) in 10 mL ampoules (Hameln Pharmaceuticals Ltd., Gloucester, UK). Heparin sodium flushing solution 100 I.U./mL (200 units in 2 mL) (Wochhardt UK Ltd., Wrexham, UK). Isoflurane (Abbott Laboratories, Illinois, US). Kinesiology Sports tape (95% cotton, 5% spandex, 5 × 500 cm) (Proworks Corporation, Corvallis, USA). Liquid silicone rubber (DDR-4320) was obtained from Nusil Technology (Buckinghamshire, UK). Ultrapure water was obtained using a water purification system from Elga PURELAB DV 25, Veolia Water Systems, Dublin, Ireland.

2.2. Fabrication and characterization of antiretroviral nanocrystals

2.2.1. Fabrication of nanocrystals (NCs)

NCs of RPV and CAB were prepared in a top-down approach by wet bead milling employing a rationalized small-scale system (Fig. 1 (A) using previously described protocols [22]. A combination of the polymers PVA 9–10 kDa and PVP 58 kDa was chosen as the medium since these stabilize the NCs during the milling process, act as cryoprotectants during lyophilization and provide a biocompatible matrix for dissolving MAPs. The rationalized parameters were as follows: 10 mL snap top glass vial, 12 g ceramic milling beads (0.1–0.2 mm), 0.25 g crude drug (RPV or CAB), aqueous solution of PVA 9–10 kDa and PVP 58 kDa (each at 2%, *w*/w), and two magnetic stir bars (8 × 25 mm) for agitation at 206 rcf. The magnetic stir plate was set at an angle of 75°, and samples were milled for 24 h. NCs of RPV and CAB were lyophilized to concentrate the respective NCs in their matrix. Prior to lyophilization, freshly prepared NCs were separated from ceramic milling beads via filtration through a 200-mesh nylon sieve. For reproducibility, 4 mL of NCs was removed

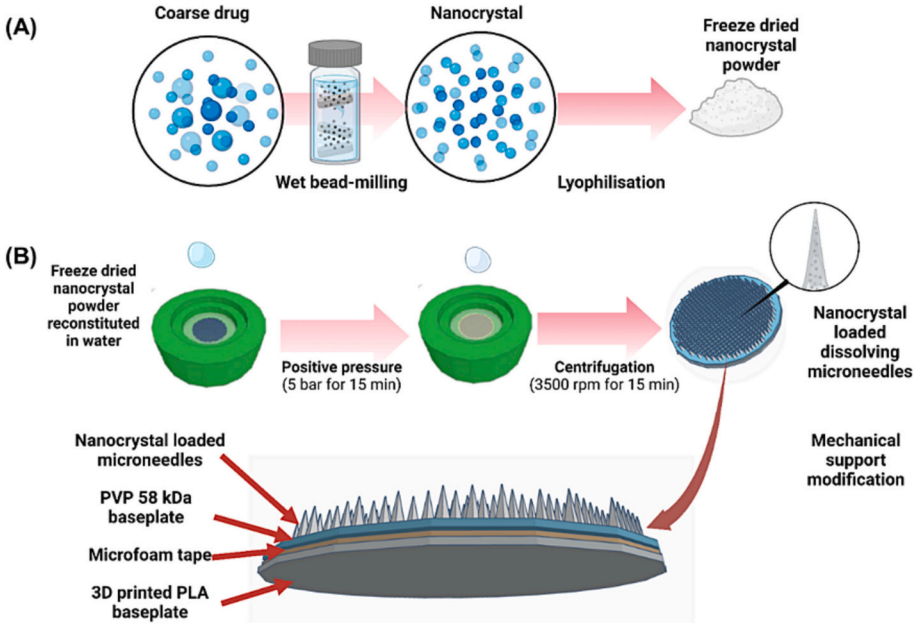

Fig. 1. Representative images of (A) NC manufacturing process for both RPV and CAB; (B) manufacturing process of multilayered MAPs loaded with RPV or CAB NCs.

from each milling vial and filtered through the sieve into a 12 mL SpeedMixer™ poly (propylene) cup. The sieve was then washed with 1 mL aqueous stabilizer solution, a combination of 2% (*w*/w) each of PVA 9–10 kDa and PVP 58 kDa. Drug content was analyzed using a previously developed and validated HPLC-UV method. Samples were lyophilized following a previously reported protocol [23].

2.2.2. Dynamic light scattering (DLS)

NCs were characterized regarding their particle size and distribution via dynamic light scattering and their zeta potential via phase analysis light scattering using a NanoBrook Omni Particle size and zeta potential analyzer. Samples were placed into a poly(styrene) cuvette cell and diluted with deionized water. After equilibration at 25 °C for 180 s, samples were analyzed regarding their particle size and distribution at a scattering angle of 90° for 180 s. For zeta potential analysis, a solvent-resistant electrode was placed into the samples, and the electrophoretic mobility of NCs was measured at a 15° detection angle. All samples were measured in triplicate.

2.2.3. Attenuated total reflectance - Fourier transform infrared spectroscopy (ATR-FTIR), differential scanning calorimetry (DSC) and X-ray diffraction analysis (XRD)

To compare the fundamental molecular vibrations of RPV and CAB and their physical mixtures and lyophilized NCs, ATR-FTIR was performed using an Accutrac FT/IR-4100TM Series spectrometer equipped with a MIRacleTM diamond ATR accessory. Analysis was performed with a resolution of 4.0 cm^{-1} and a gain of 8 over a range of 400–4000 cm^{-1}. To further examine possible interactions, DSC was employed. Accurately weighed samples with weights between 2.76 and 9.54 mg were placed in an aluminum pan and scanned on a Q100 Differential Scanning Calorimeter with an empty aluminum pan as a reference. Each analysis was conducted within a temperature range from ambient to 300 °C at a heating rate of 10 °C/min under nitrogen flow (50.0 mL/min). To confirm the crystallinity of RPV and CAB in their respective NCs after lyophilization, XRD patterns were obtained using a MiniFlex II Desktop Powder X-ray diffractometer. Samples were gently consolidated on a glass holder with a 0.2 mm depression. Measurements were performed at a voltage of 30 kV and a current of 15 mA. Scanning was performed in an angular range of 3–60° 2theta (2θ) with a scanning speed of 2.0°/min and a sampling width of 0.03° in continuous mode. For all measurements, physical mixtures were prepared by thoroughly mixing either RPV or CAB with PVA 9–10 kDa and PVP 58 kDa in a ratio of 50:25:25 using a mortar and pestle.

2.3. Design and fabrication of nanocrystal (NC)-loaded MAPs

Polymeric MAPs were fabricated via micro moulding. Previously developed silicone micromoulds [24] were employed to obtain MAPs with 600 pyramidal MNs in a circular setup on an area of 0.75 cm^2, an MN height of 750 μm, a base of 300 × 300 μm and an interspacing at the base of 50 μm. The total MN volume was 13.5 mm^3. Starting from a two-layer MAP design with a high molecular weight PVP (360 kDa) backing layer as previously employed [23,25], the design was refined to achieve quick MN separation and an increased potential for consumer acceptance. For this, a multilayer approach with a 3D-printed backing layer was taken. The first layer was prepared from lyophilized NCs of RPV or CAB. To achieve an aqueous polymeric blend with a viscosity suitable for casting, 700 μL deionized water was added to each sample, followed by rapid mixing in a SpeedMixer™ at 3500 rpm for 5 min. To eliminate air bubbles, containers were centrifuged at 1096 rcf for 5 min followed by a second mixing step at 3500 rpm for 5 min to distribute NCs within the gel evenly. Approximately 100 μL of the now homogenously mixed polymer blend was applied to each micromould and spread out evenly. After application of a pressure of 5 bar for 15 min using a pressure chamber, the excess formulation was carefully removed from each mould with a spatula, and the first layer was dried under temperature-controlled conditions at 20 °C for 2 h. The influence of MAP fabrication on the effective diameter of drug nanocrystals was determined via dynamic light scattering. For analysis, ten individual MNs were dissolved in deionized water.

For improved intradermal MN implantation, multilayered MAPs were designed (Fig. 1 (B)). A thin intermediate layer of 200 μL of an aqueous blend of 30% (*w*/w) PVP 58 kDa was cast on top of the first layer. After centrifugation at 1096 rcf for 30 min, MAPs were dried under temperature control for 2 d, carefully demoulded, and visually inspected using a Leica EZ4 W stereo microscope with an integrated camera and a Tabletop TM 3030 SEM (Hitachi High-Technologies Corporation, Tokyo, Japan). MAPs were stored under a vacuum in 24-well

microplates at room temperature until further use. For mechanical support, a backing layer was engineered employing Microfoam™ surgical tape, double-sided tape and a 3D-printed PLA disk. PLA disks were designed using Tinkercad® (Autodesk Inc., San Rafael, CA, USA) computer-aided design software and printed with an Ultimaker 3 3D printer using Cura® software (Ultimaker, Geldermalsen, Netherlands). Disks had a diameter of 15 mm and a thickness of 1 mm and were attached to Microfoam™ tape with double-sided tape that was cut in the appropriate dimensions (circles with a diameter of 15 mm). Prior to MAP testing, each MAP was assembled with one backing layer. For in vivo studies, Microfoam™ tape was cut into rectangles (2.5 × 3 cm) to allow for the fixation of MAPs on the back of animals.

2.4. Drug content uniformity

To determine the RPV or CAB content of MAPs, including the uniformity across individual MAPs and between different MAPs, MAPs were cast as described above with a thin PVP 58 kDa layer. However, this was only dried for 18 h to ensure higher flexibility. Upon demoulding, rows of ten MNs each were cut off from the array using a scalpel (visualization under stereo microscope). Each row was dissolved in 0.5 mL of deionized water (vortexing for 1 min). To extract the drugs and for precipitation of polymers, 0.5 mL acetonitrile was added, followed by vortexing for 1 min and centrifugation at 16,163 rcf for 10 min. To achieve an analyte concentration within the range of the analytical method, 0.5 mL of the supernatant was taken off and further diluted with 0.5 mL acetonitrile. After centrifugation at 16,163 rcf for 10 min, samples were analyzed using UV-HPLC. To assess within-MAP content uniformity, three rows of 10 MNs each were taken from different sides of individual MAPs. This was repeated for three different MAPs to evaluate between-MAP content uniformity.

2.5. Robustness and insertion characteristics

Compression test was performed for RPV- and CAB-loaded MAPs to evaluate the MNs height reduction after a compression test. This is an indicator of their robustness and is related to the mechanical strength of the materials of which the MNs are composed. This test was performed according to [26,27] using a TA. XT2 Texture Analyzer in compression mode. MAPs were positioned against a flat aluminum block. Then, the cylindrical probe (contact area 1.5 cm^2) moved vertically downward at a speed of 0.5 mm/s, compressing the MAPs. The MNs height of each side of the sample was measured before and after the test using a stereo microscope. The percentage of height reduction was determined based on the Eq. 1 [28], where H_{AC} = of an individual MN height after compression, and H_{BC} = height before compression.

Before and after compression, the length of individual MNs was measured using a stereo microscope, and the percentage reduction of MN heights was calculated following Eq. 1, where H_{BC} is the height of one individual MN before compression and H_{AC} is the height after compression.

$$Change\ in\ MN\ height = \frac{H_{BC} - H_{AC}}{H_{BC}} \bullet 100\% \quad (1)$$

A simulated insertion test of MAPs [29] was performed using an artificial skin model composed by 8 layers of Parafilm M® (thickness of 126 μm each). MAPs were compressed using the compression test described previously, however, the samples were compressed in a controlled mode (30 s/32 N) against 8 Parafilm M® using the TA. XT2 Texture Analyzer in compression mode as well. After the test the holes created were counted in each layer using a stereo microscope, and the percentage of insertion per layer determined using the Eq. 2. Additionally, MAPs were also inserted into 8 Parafilm M® layers using thumb pressure, and the results of controlled and manual force were compared.

$$Holes\ in\ Parafilm\ M = \frac{Number\ of\ holes\ observed}{Number\ of\ MNs\ per\ MAP} \bullet 100\% \quad (2)$$

In addition to using an artificial skin model, MAPs were also inserted into neonatal porcine skin (full-thickness) obtained from stillborn piglets, and the skin was prepared according protocol developed previously [23]. Then, MAPs were applied into the skin manually and the thumb force was held for 30 s. OCT was used for the visualization of MAP insertion [30].

2.6. Drug extraction from skin samples

The skin extraction protocol was described previously by [15,16] and consisted on extract the drug from the full-thickness skin samples obtained from the MAP application site. The skin samples(1 cm^2) were cut using scissors, and transferred to an Eppendorf tube (2 mL). Sequentially, 500 μL of water +1 mL of acetonitrile +2 stainless steel beads (5 mm diameter) were added in the Eppendorf tube containing the skin and homogenized using a TissueLyserLT (QIAGEN, U.K.) for 15 min / 50 oscillation per 1/s. Tissue samples were then transferred to a 15 mL falcon tube containing 3.5 mL of acetonitrile and left in the ultrasonic bath for 1 h. The last step consisted of transferring 100 uL of the supernatant to an Eppendorf tube (1.5 mL) containing 900 uL of acetonitrile, vortex for 30 s and centrifuge the samples at 16,163 rcf for 15 min. The resulting supernatant was collected and transferred to 2 mL HPLC vials, and the drugs were sequentially quantified by the described HPLC-UV method.

2.7. Ex vivo skin recovery

The procedure to determine the drug recovery of CAB and RPV from full-thickness skin consisted of spiking 50 μL of both nanocrystals reconstituted previously in water. The concentrations applied in 0.5 cm^2 of intact skin were 729 ± 19 μg of RPV and 647 ± 32 μg of CAB ($n = 6$) [3,8]. Subsequently, the skin was cut into small pieces using scissors, homogenized, and the drugs were extracted using 5 mL of acetonitrile [10]. The same procedure was repeated using 5 mL of organic solvent (acetonitrile) as a control ($n = 6$). The skin recovery percentage was calculated in relation to samples without skin exposed to the same conditions.

2.8. Ex vivo skin deposition

Ex vivo in-skin deposition of RPV and CAB was investigated at designated time points employing full-thickness neonatal porcine skin. To ensure stable and reproducible conditions, a modified Franz cell apparatus [32] was used. Donor compartments of Franz diffusion cells were designed specifically using Tinkercad® to fit the dimensions of MAPs and printed with the Ultimaker 3 3D printer using Cura® software out of PLA. Circular sections of skin were secured with cyanoacrylate glue to the donor compartments. These were then placed onto two layers of Parafilm M® for skin support. MAPs were inserted manually with the aid of a 5 mL syringe plunger, with firm pressure held for 30 s. A cylindrical stainless-steel weight (12 g) was placed on each MAP to prevent expulsion from the skin. Donor compartments were placed onto receiver compartments. Each receiver compartment contained 12 mL PBS (pH 7.4) and was stirred at 600 rpm. The temperature was kept at 37 ± 1 °C. Franz diffusion cells were sealed with Parafilm M® to prevent evaporation. Franz diffusion cells were disassembled at designated time points, and skin was visualized using a stereomicroscope and disrupted with a scalpel. The drug was extracted from skin samples following a previously outlined protocol and analyzed using the validated UV-HPLC method. The results were calculated based on the skin recovery for each drug. Additionally, during the 24 h skin deposition experiment, samples were taken from the acceptor compartments at predetermined time points using 1 mL syringes attached to 8 cm stainless-steel needles. The

taken volumes (200 μL) were replaced immediately with an equal volume of PBS (pH 7.4). Samples were diluted with 200 μL acetonitrile, centrifuged at 16,163 rcf for 10 min and analyzed using the validated UV-HPLC method.

2.9. In vivo pharmacokinetics and biodistribution study

The MAP-mediated intradermal delivery of RPV and CAB was assessed in vivo in a combined pharmacokinetics and biodistribution study. The aim was to evaluate the plasma pharmacokinetic and biodistribution profiles (by dissection) in female Sprague Dawley rats following the simultaneous application of RPV- and CAB-loaded MAPs. Intramuscular injections of commercially available long-acting NCs of RPV (300 mg/mL, Janssen Pharmaceutica, Beerse, Belgium) and CAB (200 mg/mL, ViiV Healthcare Ltd., Brentford, UK) were used as controls (Fig. 2). Prior to intramuscular injection, NCs were diluted with water for injection to achieve a concentration of 25 mg/mL each. The study was conducted in healthy, female Sprague Dawley rats ($n = 40$) aged 10–12 weeks and weighing 260 ± 23 g when commencing the experiment. Animals were acclimatized to laboratory conditions for a minimum of seven days prior to the experiment. Rats were divided into two cohorts ($n = 20$ per cohort), and each cohort was further divided into five groups ($n = 4$ per group).

The control cohort received intramuscular injections at a dose of 5 mg/kg. Each animal received one injection (50 μL containing 1.25 mg drug) into the right posterior thigh (RPV) and one injection into the left posterior thigh (CAB) at the start of the study. The second cohort received the drugs via MAP application to the back of animals. Each animal received two RPV-loaded MAPs (lower back) and two CAB-loaded MAPs (upper back). This equalled a total dose of 15 mg/kg for RPV and 18 mg/kg for CAB. Considering the ex vivo skin deposition, the assumed deposited dose was 2.88 mg/kg (720 μg) for RPV and 3.68 mg/kg (920 μg) for CAB.

One day prior to MAP application, animals of the second cohort were sedated using gaseous anesthesia (2–4% isoflurane in oxygen), and the hair on the back of the animals was shaved with electric clippers. Hair removal cream was applied after shaving to ensure complete hair removal. On the following day, MAPs were applied to the back of animals under gaseous anesthesia using firm finger pressure for 30 s. MAPs were secured in place with Microfoam™ surgical tape (part of the MAP backing layer) and a piece of Tegaderm™ tape, which was placed on top of the MAPs. Kinesiology™ tape was gently wrapped around the back and abdomen of each animal for further protection. Animals were housed individually until MAP removal to prevent them from removing or consuming the MAPs. MAPs were removed under gaseous anesthesia after 24 h, and the back of the animals was wiped with a wet cloth to remove any polymer and drug residues. The skin was visually inspected to ensure the absence of possible irritations.

For the biodistribution study, one group of animals ($n = 4$) per cohort was sacrificed at predetermined time points. The time points were set at 1, 3, 7, 10 and 28 d after drug application. Animals were culled using a CO_2 chamber followed by cervical dislocation. After blood collection via cardiac puncture, the following tissues were excised: skin at MAP application sites, abdominal skin, axillary lymph nodes, external lumbar lymph nodes, iliac lymph nodes, vaginal tissue, liver, kidneys and spleen.

For the plasma pharmacokinetics study, blood samples (200 μL) were collected at predetermined time points via tail vein bleeds ($n = 4$ per cohort per time point) into heparinized tubes (10 μL). The time points were set at 4 h, 1, 2, 3, 5, 7, 10, 13, 16, 21 and 28 d after drug application. Blood samples on days 1, 3, 7 and 10 were collected from the respective groups that were to be sacrificed on those days. All other blood samples were collected from the two groups that were to be sacrificed after 28 d (the end point of the study).

The heparinized blood samples were submitted to centrifugation process (2000 *g* for 10 min at 4 °C) to obtain the plasma. The organs harvested from the animals (livers, kidney, spleens, lymph nodes, vaginal tissue, skin) were cleaned using PBS (pH 7.4). Sequentially, a scalped was used to disrupt the organs mechanically. CAB and RPV were extracted using acetonitrile [31] and analyzed (HPLC–MS) following a previously published procedure [31].

The lymph-targeted drug delivery, the percentage drug targeting efficiency (%DTE), and direct transport percentage (%DTP), and the biodistribution in the organs, tissue and plasma were calculated accordingly [10,21] using the Eqs. 3 and 4:

$$\%DTE = 100\% \bullet \frac{c_{MAP}(LN)/c_{MAP}(P)}{c_{IM}(LN)/c_{IM}(P)} \tag{3}$$

$$\%DTP = 100\% \bullet \frac{c_{MAP}(LN) - \frac{c_{IM}(LN)}{c_{IM}(P)} \bullet c_{MAP}(P)}{c_{MAP}(LN)} \tag{2}$$

Due to limited time points for the biodistribution study, the mean concentration levels obtained in plasma and the respective lymph nodes at each time point were compared instead of comparing the AUCs. %DTE was calculated following Eq. 3, based on mean concentrations achieved at each time point in lymph nodes (LN) and plasma (P) after

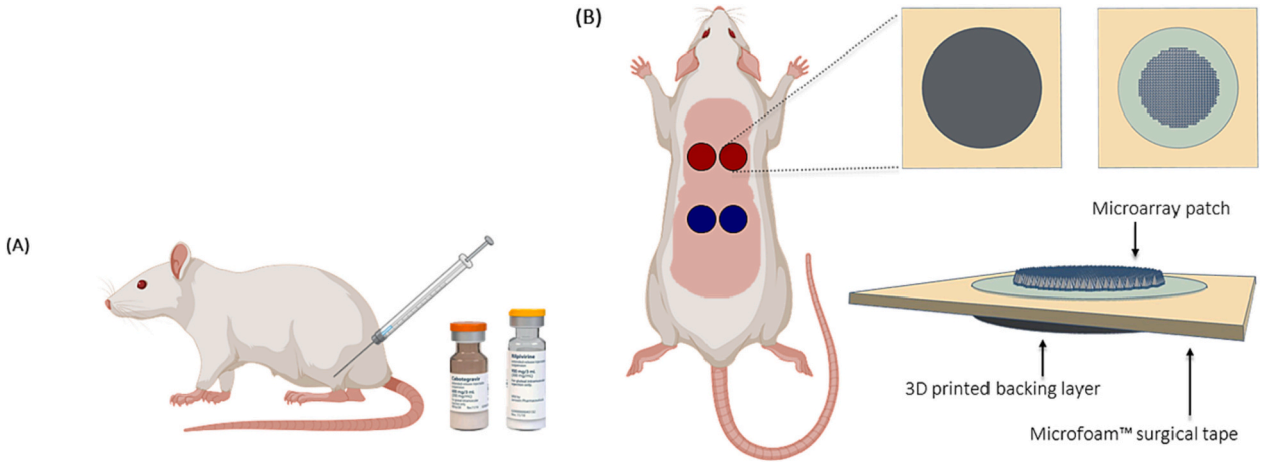

Fig. 2. Schematic representation showing the two different cohorts. (A) Intramuscular injection of commercial long-acting nanosuspensions into the right (rilpivirine) and left (cabotegravir) posterior thigh of animals of the first cohort. (B) Microarray patch (MAP) application to animals of the second cohort. Rilpivirine-loaded MAPs were applied to the lower back of the animals (blue), and cabotegravir-loaded MAPs were applied to the upper back (red). (For interpretation of the references to colour in this figure legend, the reader is referred to the web version of this article.)

intramuscular injection (C_{IM}) or MAP application (C_{MAP}). % DTE represents relative exposure of the lymph nodes to the drug after MAP application compared to intramuscular injection. A value >100% shows superior lymph-targeted delivery via MAPs. %DTP represents the percentage of the administered dose that reached the lymph nodes after MAP application compared to intramuscular injection. %DTP values can vary from -∞ to 100%. A positive value shows effective lymph-targeted delivery.

The combined in vivo pharmacokinetics and biodistribution under the Procedure Project License (PPL) 2903 approved by the Committee of the Biological Services Unit, Queen's University Belfast, and the procedures were conducted by trained licensed scientists under Procedure Individual License. (PIL) 1747, 1892, 2056, 2058 and 2059. Principles of the replacement, reduction and refinement were followed as well as the policy of the European Convention for the Protection of Vertebrate Animals used for Experimental and Other Scientific Purposes, and the Federation of European Laboratory Animal Science Associations (FELASA) [33].

2.10. Pharmaceutical analysis

CAB and RPV in vitro samples were analyzed using a HPLC previously validated [16] according to the ICH guidelines on the validation of analytical procedures [34], using an HPLC-UV (Agilent, 1220 Infinity LC system). The mobile phased consisted on deionized water + TFA 0.1% (*w*/w) and acetonitrile (19:81), flow rate 0.3 mL/min, volume of injection 30 μL, run time 13 min, wavelength of 257 nm, column temperature 40 °C, and the column consisted an Apex Scientific Inertsil ODS-3 column, 5 μm particle size, 250 mm length x 4.6 mm internal diameter. The data was accessed using an Agilent Chemstation® Software was used for chromatographic analysis. In vivo samples were analyzed employing a fully validated HPLC–MS method as previously described [31].

2.11. Statistical analysis

Statistical analysis was performed using GraphPad Prism® 7 (GraphPad Software, San Diego, CA, USA). An unpaired *t*-test was performed to compare the statistics of two groups. Comparison of multiple groups were accessed via ANOVA (analysis of variance) combined with Tukey's post hoc test. In all cases, $p < 0.05$ denoted statistical significance. The ROUT method ($Q = 1\%$) was used to identify outliers.

3. Results and discussion

3.1. Fabrication of antiretroviral NCs via wet bead-milling

To prepare NCs, a range of formulations were tested (Fig. S1) before reaching the final NC composition, which consisted of 0.25 g crude drug (RPV or CAB), PVA 9–10 kDa and PVP 58 kDa (each at 2%, *w*/w) aqueous solution. Both RPV and CAB NCs were produced separately by the milling technique. The wet bead-milling process was first rationalized for the production of RPV NCs approaching a particle size close to 100 nm. To assess the effect of the milling bead diameter on the particle size of NCs, many parameters were tested, such as bead-milling size, milling time and different angles. Finally, the final NCs were rationalized under the same conditions for RPV and CAB (separately) using a 10 mL snap top glass vial, 12 g ceramic milling beads (0.1–0.2 mm) (Fig. S2) and two magnetic stir bars (8 × 25 mm) using agitation at 1500 rpm.

The magnetic stir plate was set at an angle of 75°. The particle size of the RPV NCs produced was 239 ± 2 nm ($n = 3$). When reducing the amount of beads to only 30%, RPV NCs had a particle size of 168 ± 2 nm ($n = 9$). The polydispersity index was 0.178 ± 0.019 ($n = 9$), and the zeta potential was 1.58 ± 1.76 mV ($n = 9$). These parameters were employed for all further experiments as well as the fabrication of CAB NCs. These had a particle size of 172 ± 6 nm ($n = 9$), a polydispersity index of 0.174 ± 0.015 (n = 9) and a zeta potential of 7.17 ± 4.22 mV (n = 9).

3.1.1. Effect of lyophilization on the particle size of antiretroviral NCs

The polymers PVA 9–10 kDa and PVP 58 kDa were added for stabilization of NCs during fabrication and acted simultaneously as cryoprotectants during lyophilization. The particle size of RPV NCs did not change significantly during lyophilization ($p = 0.8330$); it was 168 ± 2 nm (n = 9) before lyophilization and 169 ± 3 nm (n = 9) after lyophilization and reconstitution. For CAB NCs, the particle size increased slightly ($p < 0.0001$), from 172 ± 6 nm (n = 9) to 190 ± 6 nm (n = 9). The dynamic light scattering reports for RPV and CAB NCs are shown in Fig. S3 and Fig. S4, respectively. Even though the particle size was, in all cases, above the desired size of 100 nm, a considerable number of nanocrystals were sized <100 nm for both RPV and CAB [16,35,36].

3.1.2. Surface morphology

The surface morphology of powdered RPV and CAB, as well as their respective lyophilized NCs, was visualized via SEM. In Figure, individual crystals of unprocessed RPV and CAB powder of varying shape and diameter, in a range of approximately 1–25 μm, are visible. Compared to the bulk powders, the surface of lyophilized samples was more porous, without individual micron-sized crystals visible (Fig. 3 (E) and (G)). At a higher magnification of 2000×, individual white dots were observed in the lyophilized RPV (Fig. 3 (F)) and CAB (Fig. 3 (H)) nanosuspensions. As these were not present in the lyophilized polymer solution (Fig. S5)), they were assumed to be individual RPV and CAB NCs.

3.1.3. Attenuated total reflectance Fourier transform infrared spectroscopy (ATR-FTIR), differential scanning calorimetry analysis (DSC) and powder X-ray diffraction (XRD)

ATR-FTIR was used to analyze the fundamental molecular vibrations of RPV, CAB, PVA 9–10 kDa, PVP 58 kDa, as well as their respective physical mixtures and lyophilized NCs, to identify possible interactions between the compounds. The skeletal structural formulas of the analyzed substances and the obtained ATR-FTIR spectra are displayed in Fig. 4 (A, B, C and D). The spectrum of RPV showed characteristic bands at approximately 805 cm^{-1} (aromatic), 1411 cm^{-1} (pyrimidine ring), 2215 cm^{-1} (C≡N), and 3316 cm^{-1} (N—H) (Fig. 4 (E)). CAB displayed a small band at approximately 3076 cm^{-1} (O—H), a further band at 1652 (C=O) and a characteristic fingerprint region due to the complexity of the molecule (4 (F)). PVA 9–10 kDa showed a characteristic broad band at approximately 3338 cm^{-1} (O—H) and a further small band at 2935 cm^{-1} (C—H), which was also present in PVP 58 kDa, next to a band at 1660 cm^{-1} (C=O). The characteristics of the spectra of RPV and CAB were still present in the spectra obtained by analyzing the respective physical mixtures and lyophilized NCs, and no additional peaks appeared. This indicated that no chemical interactions occurred while processing the therapeutic agents into nanocrystals.

The DSC thermograms of RPV, CAB, PVA 9–10 kDa, PVP 58 kDa and their respective physical mixtures and lyophilized NCs are shown in Fig. 4. The pure RPV powder exhibited two endothermic peaks at 244.41 °C and 258.3 °C and one exothermic peak at 248.6 °C. Different polymorphic forms of RPV have previously been observed 27, and the DSC profile indicates the presence of an enantiotropic pair 28. During the scans, endothermic peaks were observed in both the physical mixture and the lyophilized nanosuspension at 239.3 °C and 231.8 °C, respectively. The presence of only one peak, the slight shift in temperature and diminished peak size might be attributed to the early melting of the stabilizers and partial amorphisation of the drug during the analysis. For CAB, one distinctive endothermic peak was observed at 251.6 °C. This again shifted slightly in the physical mixture and the lyophilized nanosuspension to 248.1 °C and 241.7 °C, respectively. The melting point of PVA (9–10 kDa) was detected at 176.9 °C, and that of PVP (58 kDa) was detected at 110.4 °C. The endothermic peaks were,

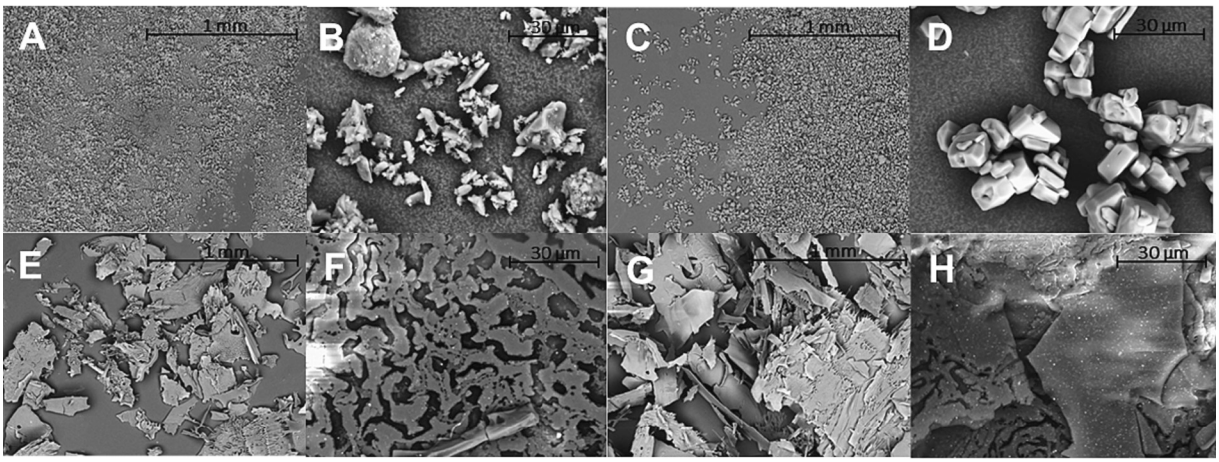

Fig. 3. Scanning electron microscopy images of powdered rilpivirine at magnifications of (A) 100× and (B) 2000× and of powdered CAB at magnifications of (C) 100× and (D) 2000×. (E) RPV nanosuspension (100×), (F) RPV nanosuspension (2000×), (G) CAB nanosuspension (100×), (H) CAB nanosuspension (2000×).

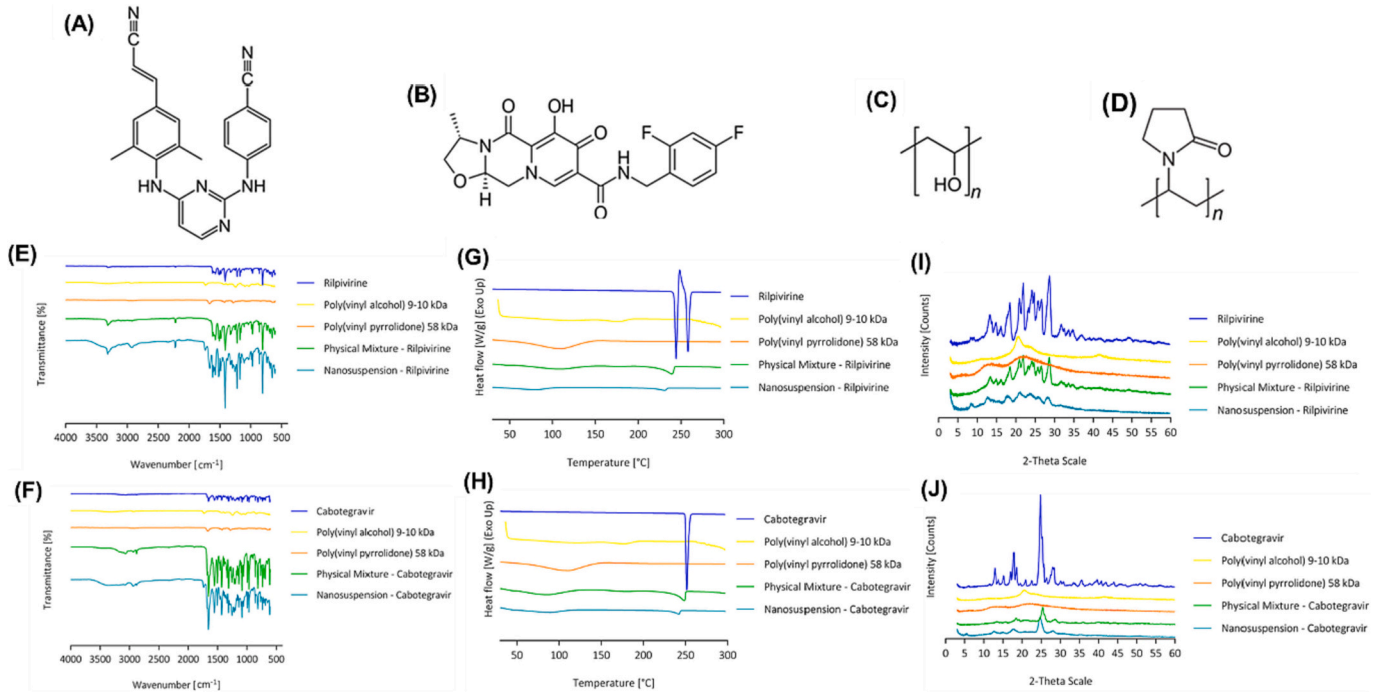

Fig. 4. Skeletal structural formulas of (A) RPV, (B) CAB, (C) poly (vinyl alcohol) (PVA 9–10 kDa) and (D) poly (vinyl pyrrolidone) (PVP 58 kDa). (E) ATR-FTIR spectra of RPV and (F) CAB their physical mixture, lyophilized nanosuspension and their polymeric components separately PVA 9–10 kDa and PVP 58 kDa. (G) DSC thermograms of RPV and (H) CAB, their physical mixture and lyophilized nanosuspension and their components PVA 9–10 kDa and PVP 58 kDa. (I) XRD of RPV and (J) CAB and their respective physical mixtures and lyophilized nanosuspensions as well as PVA 9–10 kDa and PVP 58 kDa.

however, not well defined. The polymer peaks shifted slightly in the physical mixtures with RPV or CAB and became less defined. In the NCs, the endothermic peak of PVA 9–10 kDa was not detectable. However, due to the porous character of the lyophilized NCs, only small amounts of powder could be placed in the aluminum pans, which might explain the diminished peaks.

The X-ray patterns of the RPV and CAB powder samples showed clearly defined peaks, confirming their crystallinity (Fig. 4). The diffractogram of RPV showed distinctive peaks at 2-theta values of 13.44°, 18.42°, 20.90°, 21.90°, 24.12°, 26.66° and 28.72°. CAB exhibited sharp peaks at 12.92°, 17.82°, 24.84° and 28.06°. Neither PVA 9–10 kDa nor PVP 58 kDa showed clearly defined peaks due to the amorphous characteristics of these polymers. However, an increase in the diffraction pattern could be observed at 20.48° and 41.54° for PVA 9–10 kDa and at 13.62° and 22.02° for PVP 58 kDa. In the physical mixtures and lyophilized NCs of RPV and CAB, all distinctive peaks were retained but slightly diminished, which might be attributed to the presence of amorphous polymers. Nevertheless, the presence of distinctive peaks in the lyophilized NCs indicated the absence of phase changes or chemical interactions and confirmed the crystallinity of RPV and CAB NCs.

3.2. Fabrication of NC-loaded MAPs

3.2.1. NC-loaded MAPs with high molecular weight poly (vinyl pyrrolidone) backing layers

The fabrication process of RPV or CAB nanocrystal-loaded MAPs with PVP (360 kDa) backing layers was rationalized to obtain fully formed MAPs without air bubbles. After initial reconstitution and

mixing of NCs, the gels had the appearance of thick foam. When immediately casting this gel, the first MAP layer was only partly formed, and the drugs were not evenly distributed due to the presence of air bubbles in individual MNs. Thus, an additional centrifugation and mixing step was introduced, eliminating possibly entrapped air. The amount of deionized water added for reconstitution was adjusted to achieve a slightly viscous gel. This had to be liquid enough for even application to MAP moulds but viscous enough for easy removal of excess formulation and high drug content in MNs. Demoulded MAPs were fully formed, and NCs were only visible in the MN shafts (Fig. S6).

3.2.2. Design and fabrication of NC-loaded MAPs with multilayered backing layers

For improved intradermal MN implantation, multilayered MAPs were designed. In the first approach, the 3D printed PLA disk was placed immediately onto the cast PVP (58 kDa) layer. However, this process involved long periods of drying (up to three days), and adhesion between the cast layers and the PLA disk was poor (Fig. S7).

The backing layer was improved by adding Microfoam™ surgical tape and double-sided tape and only attached after MAPs were fully dried. The foamy characteristics of the Microfoam™ tape evened out any irregularities of cast MAPs, ensuring strong mechanical support. Representative light microscopic and SEM images of RPV and CAB NC-loaded multilayered MAPs are shown in Figure. MAPs were fully formed, with NCs clearly visible in the MN shafts and a visible difference in surface structure between the drug-loaded first layer and the PVP (58 kDa) intermediate layer.

3.2.3. Determination of drug content

The RPV or CAB content of MAPs, including the uniformity across individual MAPs and between different MAPs, was determined by dissolving 10 individual MNs in deionized water, followed by drug extraction and RP-HPLC analysis. The drug content of RPV-loaded MAPs was 1.9 ± 0.1 mg per MAP ($n = 9$, analyzed 3 times for 10 individual MNs from 3 different MAPs). The drug content of CAB-loaded MAPs was 2.2 ± 0.4 mg per MAP (n = 9, analyzed 3 times for 10 individual MNs from 3 different MAPs). Drugs were found to be evenly distributed throughout the individual MNs of MAPs (no significant difference, $p > 0.05$).

3.2.4. Effect of casting process on NC characteristics

The particle size and distribution of RPV and CAB NCs after casting of MAPs followed by dissolution in deionized water was analyzed. RPV NCs had an effective diameter of 159 ± 3 nm ($n = 9$) and a polydispersity index of 0.181 ± 0.017 (n = 9). Compared to the lyophilized NC (169 ± 3 nm (n = 9), item 2.1., the particle size decreased slightly ($p < 0.0001$). The CAB NCs had an effective diameter of 201 ± 5 nm (n = 9) and a polydispersity index of 0.193 ± 0.015 (n = 9). Compared to the lyophilized NC (190 ± 6 nm (n = 9), the particle size increased slightly ($p < 0.0013$).

3.2.5. Mechanical characterization

Compression tests were conducted to determine the percentage reduction in height of individual MNs on MAPs, thus giving an indication of their robustness. These tests were only performed for MAPs with a PVP (360 kDa) backing layer because the formulation for the first (drug-loaded) layer was the same for multilayered MAPs. After application of a force of 32 N/MAP for 30 s, the height of RPV-loaded MAPs was reduced by 9.8 ± 6.3% (mean ± SD, $n = 48$, 16 individual MNs measured on three different MAPs). CAB-loaded MAPs were compressed by 6.2 ± 5.9% (mean ± SD, n = 48, 16 individual MNs measured on three different MAPs) of the total MN height of 750 μm. Both MAPs showed <10% height tip reduction, indicating that the MNs developed are strong enough to penetrate the skin [37].

3.2.6. Evaluation of insertion characteristics

The insertion of RPV or CAB-loaded MAPs (Figs. 4 A – D) into an artificial skin model [29], consisting of eight Parafilm M® layers with a thickness of 126 μm each, was evaluated. MAPs with a 360 kDa PVP backing layer were inserted using a controlled force of 32 N (Fig. 5 (E)). Multilayered MAPs were inserted using either a controlled force of 32 N or thumb pressure (Fig. 5 (F)). In all cases, MAPs pierced the first Parafilm M® layer to 100 ± 0% ($n = 3$) and inserted down to the third layer of Parafilm M®, which equals 50.8% of the total MN height. Only RPV-loaded multilayered MAPs did not pierce the third layer when using a controlled force of 32 N. Even in the second layer, the insertion of these MAPs was significantly less at 32 N compared to thumb pressure ($p = 0.0072$). Comparing the manual insertion of multilayered MAPs with the insertion of MAPs with a 360 kDa backing layer at 32 N, no significant difference could be observed ($p > 0.2556$). For CAB-loaded MAPs, there was no significant difference in the percentage of holes created in the first and second layers ($p > 0.5549$). When looking at the third layer, multilayered MAPs and MAPs with a 360 kDa PVP backing layer had comparable insertion at 32 N ($p = 0.3345$). The results of this study also indicated that manual insertion using thumb pressure was superior to insertion at a controlled force using the Texture Analyzer ($p < 0.0001$).

3.2.7. Ex vivo skin recovery

The amount of RPV detected in control samples was 729 ± 19 μg compared to 695 ± 8 μg in skin samples ($n = 6$). This equals a percentage recovery of 95%. For CAB, 647 ± 32 μg was detected in control samples and 567 ± 30 μg in skin samples (n = 6). This equated to a percentage recovery of 88%.

3.2.8. Ex vivo in-skin deposition

Ex vivo in-skin deposition of RPV-loaded MAPs with a PVP (360 kDa) backing layer and of RPV- or CAB-loaded multilayered MAPs at designated time points was investigated. Additionally, during the 24 h setup, samples were taken from receiver compartments of Franz cells and analyzed. Although a slight increase in the amount of drug in receiver compartments was detected over time for both drugs, the results were below the lower limit of quantification of the analytical method and, thus, not considered further.

After 24 h, the amount of RPV deposited in skin for RPV-loaded MAPs with a PVP (360 kDa) backing layer was 202 ± 48 μg/0.75 cm^2 (n = 6), equaling a deposition of only 10.6% of the total drug load of 1.9 mg. The aim of the multilayered MAP design was to increase the drug deposition by avoiding the formation of a viscous gel upon MN dissolution. After application for 24 h, the deposition of RPV had almost doubled to 19.1% (366 ± 139 μg/0.75 cm^2) of the total drug load located in the skin. Previous studies [16] were able to deliver 110.62 ± 18.63 μg/0.49 cm^2 using a pyramidal MAP design (19 × 19 needle density; 0.49 cm^2, 500 μm height; 300 μm base width; and 30 μm interspacing) and 170.26 ± 15.25 μg/0.5 cm^2 using an MAP with a pyramidal tip design with a cuboidal base (16 × 16 needle density, 0.5 cm^2, 900 μm height (300 cuboidal base +600 pyramidal tip); 300 μm base width; and 100 μm interspacing). Normalizing the area, the new patches developed here would deliver 244 μg/0.5 cm^2, which is slightly higher than previous studies. All results are displayed in Table 1. Multilayered MAPs left only a small amount of polymer residue on the skin, which could be easily removed with a wet cloth. The deposited drug could be clearly seen in the skin, not only in the holes created by the MNs but also in the surrounding tissue (Fig. 6).

This work was focused on the development of MAPs for intradermal delivery of RPV and CAB NCs with specific properties for enhanced passive lymphatic uptake. Initially, RPV and CAB were formulated as NCs in the lower nanometer range in a matrix of PVA and PVP of low molecular weights. The rationalization of the fabrication process via wet bead milling and the full characterization of NCs are described in detail in section 2.3. PVA and PVP were chosen as stabilizers during the bead-milling process, not only due to their ability to stabilize the NCs but also

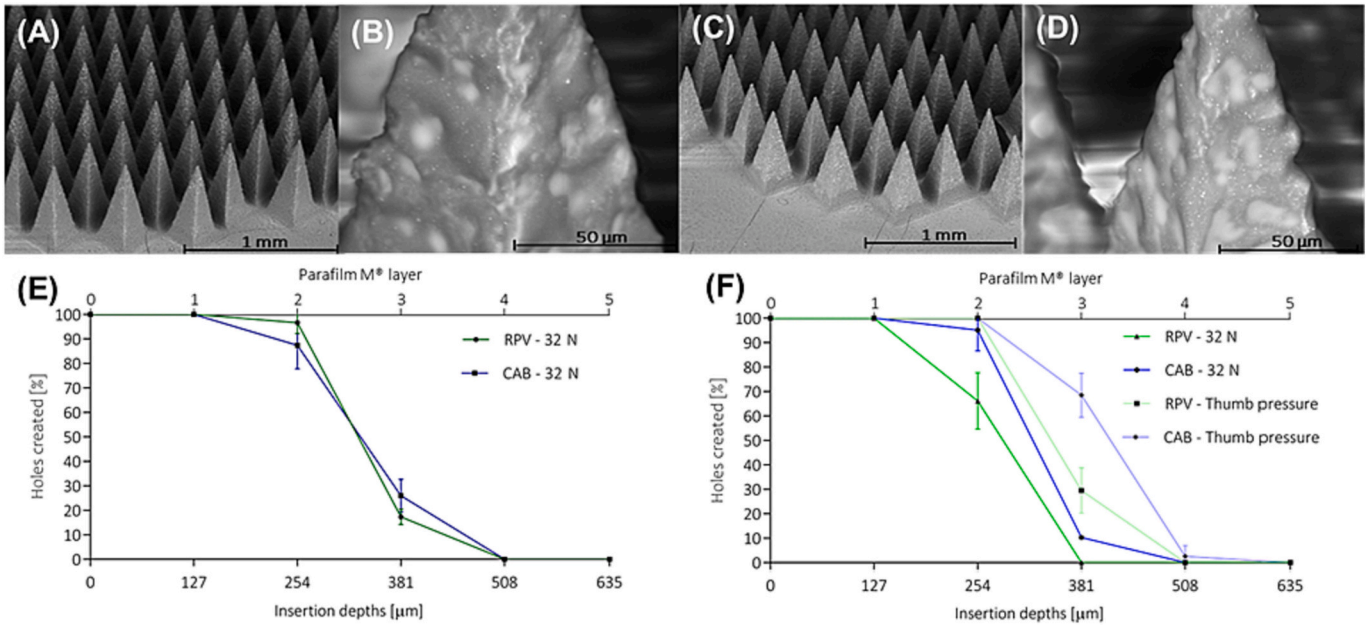

Fig. 5. (A) Scanning electron microscope (SEM) image (80×) of RPV MAP and (B) its individual RPV MN (1800×) showing individual NCs (white dots). (C) SEM image (80×) of CAB MAP and (D) its respective image (1500×) of individual CAB MN showing individual NCs (white dots). The insertion efficiency of different (RPV- or CAB)-loaded MAPs into an artificial skin model consisting of eight layers of Parafilm M® is illustrated in (E) MAPs with a backing layer of high molecular weight poly(vinyl pyrrolidone) inserted at 32 N and (F) multilayered MAPs inserted at 32 N or with manual force (thumb pressure) (means ± SD, $n = 3$).

Table 1
Ex vivo in-skin deposition in neonatal porcine skin of RPV- or CAB-loaded multilayered MAPs after 24 h. Displayed are the actual drug deposition values per applied MAP (means ± SD, $n = 6$) and the percentage drug deposition based on the total drug load of 1.9 mg/RPV-loaded MAP and 2.2 mg/CAB-loaded MAP (means ± SD, $n = 6$).

Drug	Time [h]	Drug deposition [µg]	Drug deposition [%]
RPV	24	366 ± 139	19.1 ± 7.2
CAB	24	463 ± 143	20.8 ± 6.4

because they could act as cryoprotectants during lyophilization and as a matrix in the fabrication of dissolving MAPs. This allowed for a straightforward fabrication process without the addition of other excipients. The advantage of using low molecular weight polymers was that they can be cleared by the kidneys and, thus, do not accumulate in the body [38]. Indeed, the plasma half-life of low molecular weight PVA after intravenous administration is short, at only 90 min [39]. This is of particular importance considering that the treatment of HIV will require repeated applications of MAPs over an extended period, and accumulation of excipients should be avoided. Furthermore, the combination of PVA and PVP produces MAPs with high robustness due to the potential formation of hydrogen bonds between the hydroxyl groups of PVA and the carbonyl groups of PVP [14,15]. As demonstrated within, MAPs made from these polymers are neither too brittle nor too flexible for insertion and dissolve within a short period of time. A novel MAP design described by Ramöller et al. [24] was chosen. Finally, the high number of individual pyramidal MNs per MAP allowed for a high drug load due to the increased total MN volume compared to other designs.

First, MAPs were cast in a two-step process in two layers with a high molecular weight PVP backing layer for support. PVP (360 kDa) has been used in previously published studies [25,35] because it can form rigid backing layers that aid the insertion of MAPs. NCs were only loaded into MN shafts with a drug-free backing layer. It could be assumed that due to the hydrophobic nature of RPV and CAB, only drugs implanted intradermally beneath the skin surface upon insertion of MAPs would be deposited in the skin, even after extended application periods. By formulating a two-layered system, drug wastage could be avoided. The drug contents of 1.9 mg and 2.2 mg for RPV- and CAB-loaded MAPs, respectively, were comparable to those previously reported for MAPs loaded with RPV [35]. The stability of NCs is of high importance considering the aim of passive lymphatic targeting. As no additional excipients were added to the lyophilized NCs for the formulation of MNs, the impact on particle characteristics was kept to a minimum. Even though the particle size of the NCs changed slightly when comparing dissolved MAPs to the lyophilized NCs, it remained below approximately 200 nm for both drugs. The robustness of MNs was assessed by application of a force of 32 N/MAP, which equals the maximum mean MAP insertion force applied by a human [40]. This resulted in a height reduction of <10% for RPV- and CAB-loaded MAPs. This reduction in height was in the same range as the results obtained for blank polymeric MAPs made from PVA and PVP, as described in section 3.2.3. (height reductions between 7% and 15%), showing that the amount of NCs incorporated into the MN matrix (approximately 45% drug, 55% polymers) did not negatively impact their robustness. The drug-polymer ratio was already chosen during NC manufacture with MAP casting in mind to achieve a high drug load while maintaining the mechanical integrity of the polymer matrix. MAPs could be evenly inserted into an artificial skin model down to 50.8% of their total MN length. Insertion into neonatal porcine skin showed that the dissolution process of MNs started 10 min after insertion, and the drug from the very tips of MNs was deposited in the skin. Longer application times increased the dissolution process. However, the polymeric backing layer started to dissolve after approximately 40 min and formed a sticky glue-like gel. Due to the hydrophobic nature of drug loaded MNs, this glue-like gel removed a large portion of the drugs from the skin upon MAP removal. When quantifying RPV in the skin after MAP application for 24 h, only 10% of the total drug load was deposited. This can be attributed to the poor separation of MNs from the partly dissolved and sticky backing layer. Furthermore, the removal of polymer residues from the skin was highly troublesome.

High in-skin drug deposition and minimal polymer residues on the skin surface after MAP removal are important, considering the production of economically viable and consumer-friendly products. Different

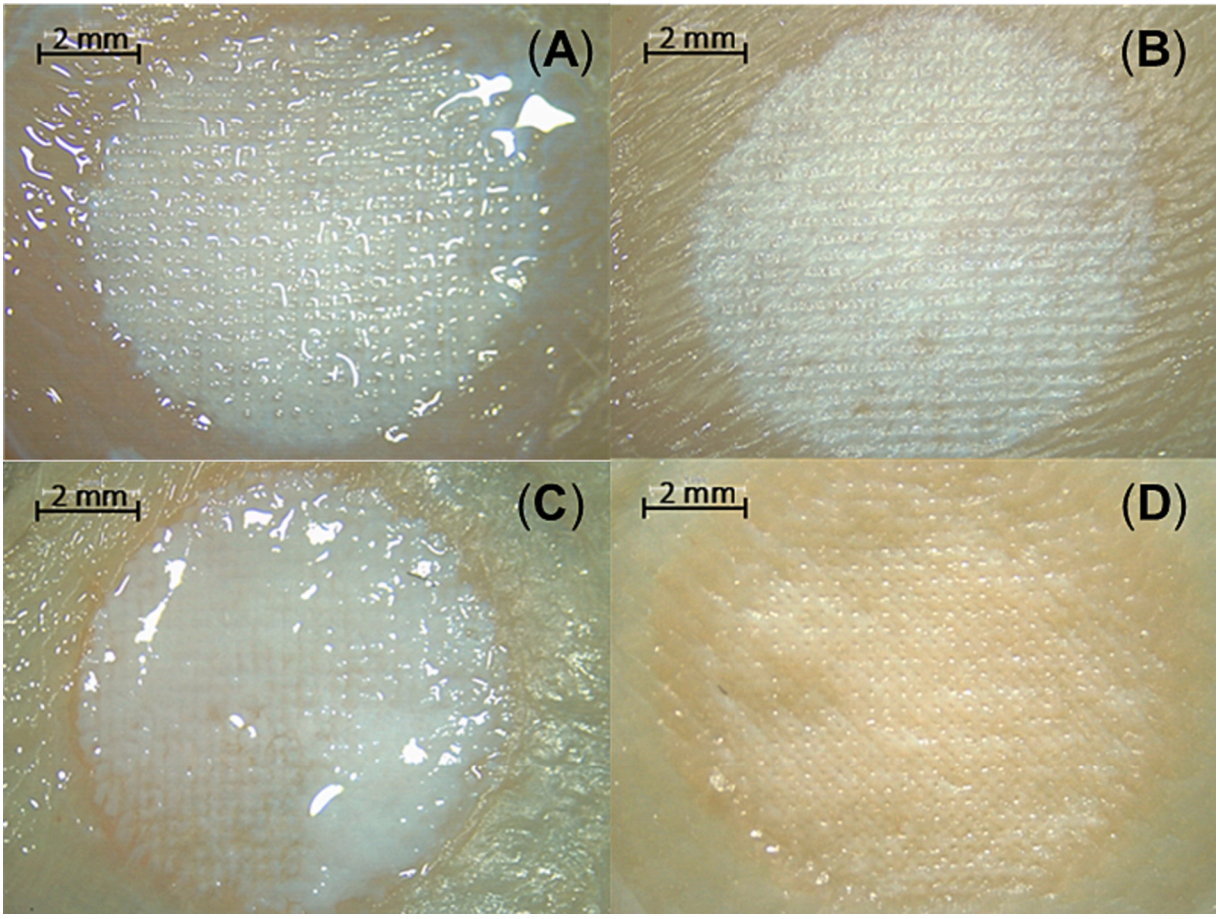

Fig. 6. Representative light microscopic images (8×) of skin samples after application of multilayered RPV or CAB MAPs during ex vivo in-skin deposition studies. Displayed are RPV deposition (A) before and (B) after removal of polymer residues and CAB deposition (C) before and (D) after removal of polymer residues.

techniques have been employed previously to achieve fast intradermal MN implantation. One of the most innovative methods includes the incorporation of an air bubble between every MN and the backing layer, allowing immediate separation of MNs from the backing layer upon insertion by application of a vertical shear force [41]. Additionally, the same research group developed MAPs with an effervescent layer between MNs and the backing layer. Upon contact with skin interstitial fluid, sodium bicarbonate and citric acid incorporated in the MAP formed carbon dioxide bubbles that weakened the mechanical integrity and led to MN separation within 1 min [42]. Both designs come with great advantages compared to the above-described high molecular weight PVP backing layer and allow for immediate implantation of MNs; however, they have certain drawbacks. The potential for reproducible production of the bubble design on an industrial scale is questionable, and MAPs are highly susceptible to damage during transportation and handling. The effervescent design is certainly more amenable to upscaling; nevertheless, humidity during storage must be controlled to prevent all MAPs from dissolving; otherwise, the needles will not be strong enough to penetrate the skin [26]. The work reported here aimed to design MAPs that would lead to fast intradermal MN implantation while keeping ease of manufacturing and handling in mind.

To achieve quick separation between MNs and their backing layer, a layer of low molecular weight PVP was cast on top of drug-loaded MNs. The formulation of this first layer was not changed. Films cast from aqueous PVP 58 kDa gels dissolve within minutes upon contact with aqueous fluid. To keep the amount of polymer to a minimum, the amount of gel cast as a second layer was adjusted to spread evenly across the MAP while keeping the layer as thin as possible. For mechanical support, a multilayered backing was developed. Microfoam™ surgical tape was chosen because of its hypoallergenic, elastic and secure adhesive properties and its ability to secure MAPs in place when applied in vivo. Due to its foam character, it was able to even out any irregularities in the PVP layer. To make the backing layer more rigid and aid insertion, a 3D printed disk (with the same dimensions as each MAP) was secured to the back of the Microfoam™ tape with double-sided tape. For in vitro studies, the tape was cut into the same dimensions as the MAPs. When looking at in vivo application, it can be cut into larger dimensions to allow for fixation of MAPs on skin. Multilayered MAPs inserted well into an artificial skin model and neonatal porcine skin. However, the Microfoam™ tape absorbed some of the force when trying to insert MAPs with a controlled force of 32 N/MAP, resulting in lower insertion compared to application with thumb pressure. When applying PBS (pH 7.4) to MAPs, MNs started to separate from their backing layers within only 10 s. This novel MAP design can thus increase the deposition of hydrophobic drugs, therefore reducing the application area needed and making the MAPs more economically viable. Furthermore, it decreases the application times and leaves minimal residues on the skin after MAP removal, resulting in a more consumer-friendly product and possibly higher user acceptability.

3.3. *In vivo pharmacokinetics and biodistribution profiles*

MAPs were applied to the back of female Sprague Dawley rats using firm finger pressure and secured in place with Microfoam™ surgical tape (part of the MAP backing layer), Tegaderm™ tape and Kinesiology™ tape. After 24 h, the Kinesiology™ tape was unwrapped carefully. Implantation of drug-loaded MNs in the skin was clearly visible. Deposited RPV appeared as white dots, whereas CAB appeared slightly

orange and was less pronounced. The intermediate PVP 58 kDa backing layers were completely dissolved in all cases. Minimal polymer residues on the skin could be easily removed with a wet paper towel. No erythema was observed at the application sites. Pictures taken during MAP removal are shown in Fig. 7 and Fig. S8.

3.3.1. In-skin deposition of rilpivirine and cabotegravir

Skin at application sites was collected from the backs of rats at 1, 3, 7 and 10 d after application. After 28 d, application sites could not be determined due to extensive hair regrowth. CAB was visible up to 7 d after application in individual animals (Fig. 7 (A)). Application sites of MAPs loaded with RPV could be clearly seen in some animals up to 21 d after application (Fig. 7 (B)).

Each application site was analyzed individually. After 1 d, 215 ± 82 μg/0.75 cm^2 RPV ($n = 8$) was deposited in the skin. Compared to ex vivo skin deposition studies in neonatal porcine skin (366 ± 139 μg//0.75 cm^2, $n = 6$, after 24 h), there was no significant difference ($p = 0.2008$). The amount detected at the application sites decreased over time, but even after 10 d, 53 ± 44 μg/0.75 cm^2 RPV (n = 8) could still be detected. For CAB, the in vivo deposition was significantly lower ($p = 0.0244$) after 24 h compared to ex vivo skin deposition studies, with 123 ± 54 μg/0.75 cm^2 (n = 8) and 463 ± 143 μg/0.75 cm^2 (n = 6), respectively. After 10 d, only 0.614 ± 0.571 μg//0.75 cm^2 (n = 8) could be detected in the skin. The results are shown in Fig. 7 (C).

For reasons of comparison, the amount of CAB detected at MAP application sites was additionally divided by the mean weight of skin samples taken from application sites (0.548 ± 0.136 μg/0.75 cm^2, n = 8) (Fig. 7). After 1, 3 and 7 d, CAB concentrations detected at application sites were significantly higher ($p < 0.0001$) than in control skin taken from the frontal abdomen of rats. However, after 10 d, there was no significant difference between CAB levels at application sites and in abdominal skin samples ($p = 0.7457$). As only traces of RPV could be detected in abdominal skin samples, no further calculations were made.

3.3.2. In vivo delivery of rilpivirine and cabotegravir

3.3.2.1. Plasma. RPV and CAB concentration levels in plasma and various organs were analyzed. In all cases, RPV results were highly variable; thus, the results obtained for organs of individual animals were reported and plotted as scatter diagrams, and no statistical or pharmacokinetic analysis was performed. Instead, individual values were compared. Plasma concentration levels above the IC_{90} of 12 ng/mL, which denoted therapeutically relevant concentrations, were delivered over a month.

After intramuscular injection of a long-acting RPV nanosuspension at a dose of 5 mg/kg, therapeutically relevant plasma concentrations were reached in three of four animals after 4 h (58 ± 36 ng/mL, $n = 4$). These were maintained over 1 d (52 ± 19 ng/mL, n = 4). After 2 d, the plasma concentrations of two animals fell below the quantification limit of the bioanalytical method. These were treated in data analysis as having RPV levels of 5 ng/mL (detection limit). In the other two animals, therapeutically relevant concentrations were achieved. After 3, 5 and 7 d, only one animal at each sample point had quantifiable and therapeutically relevant plasma concentrations. RPV traces could be detected in the plasma of all animals up to 21 d after application. No drug was detectable after 28 d.

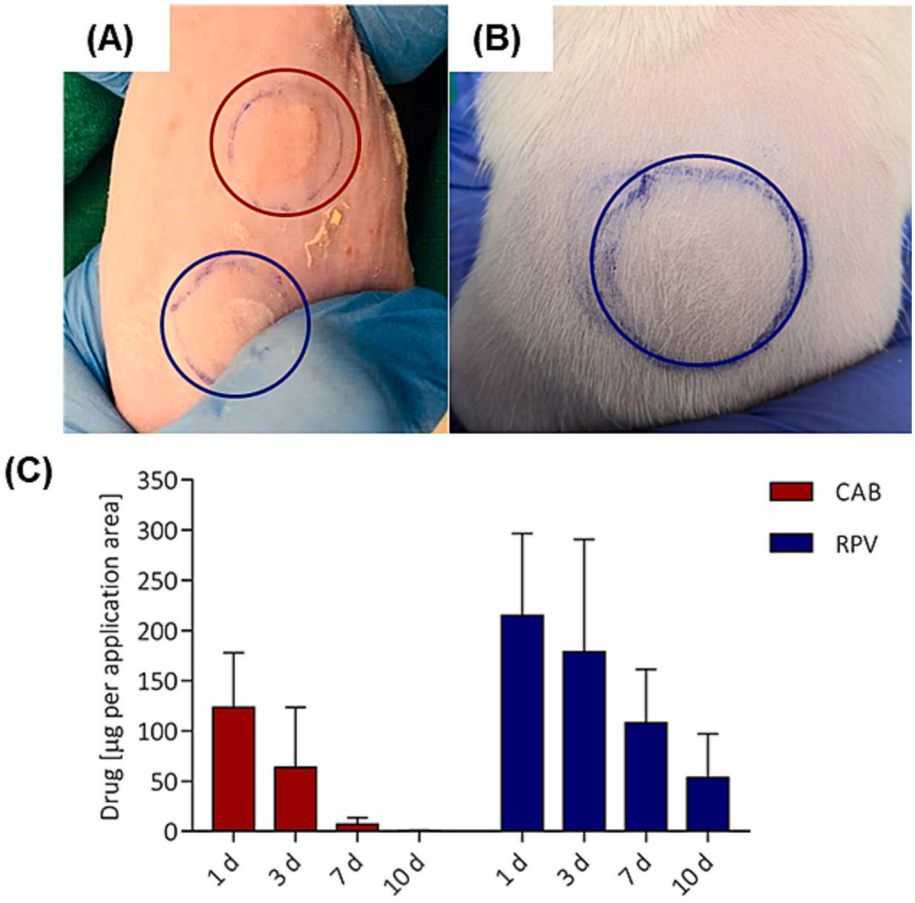

Fig. 7. (A) MAP application sites on the back of female Sprague Dawley rats 7 d after application and (B) 21 d after application. Application sites of RPV-loaded MAPs are marked in blue, and those of CAB-loaded MAPs are marked in red. (C) Intradermal drug deposition after application of CAB- or RPV-loaded MAPs to the back of female Sprague Dawley rats (means + SD, $n = 8$). (For interpretation of the references to colour in this figure legend, the reader is referred to the web version of this article.)

In the MAP cohort, RPV could be quantified for individual animals only up to 2 d after application. After 4 h, two animals had therapeutically relevant plasma levels (rat 1: 87 ng/mL; rat 4: 19 ng/mL). After 1 d, RPV could only be quantified in one animal (186 ng/mL). After 2 d, two animals had therapeutically relevant plasma concentrations (rat 2: 15 ng/mL; rat 4: 75 ng/mL). Even though the samples taken after 2 d were from the same animals as after 4 h, therapeutically relevant RPV levels were detected in varying animals. From 3 d onward, RPV traces could be detected in the plasma of all animals but were not quantified. In contrast to the intramuscular cohort, RPV could still be detected 28 d after MAP application. No pharmacokinetic analysis was performed based on the obtained results for RPV plasma concentrations due to the highly variable, and concentrations detected below the quantification limit from 3 d onward. In vivo plasma profiles are displayed in Fig. 8 (a) and (b). In this work, RPV NCs and the MAPs into which they were formulated were fabricated using PVA and PVP, and the dose applied to each rat was approx. 3.8 mg. Previous work from McCrudden et al. [12] demonstrated delivery of RPV at therapeutic plasma concentrations for 56 days in rats after application of dissolving MAPs totalling a dose of approx. 8 mg [35]. These MAPs, primarily composed of low molecular weight PVA, contained a commercially available RPV nanosuspension that was prepared using Poloxamer 188. A similar delivery profile was observed by Moffatt et al. [16] when Poloxamer 188 was used to prepare an RPV nanosuspension that was subsequently formulated into dissolving MAPs [21]. In this previous work, therapeutic levels of RPV were observed in plasma for 63 days following application of two dissolving MAPs totaling a dose of 4.48 mg.

When the findings from these studies are compared with the results obtained here, it is suggested that the particle size difference for RPV NCs developed here (169 nm), is smaller when compared with previous work published with RPV MAP NS-loaded NCs that possessed particle sizes of 300 nm [35] and 204 nm [16], respectively. Nanoparticles falling in the size range closer to 100 nm have an easy access to the lymphatic capillaries with the ability to accumulate into the regional lymph nodes [17].This can explain the lower plasma concentration of RPV and higher concentration in the lymphatic system. Comparing the present work with Moffatt [16] and McCrudden [35] studies The charge are also very important to consider as it influences the encounter between the charged particles and the interstitial matrix on the basis of electrostatic forces [17] Additionally, this impacts the residence time of the particles in the lymph nodes [43]. In this case we have positive zeta-potential whereas, our previous work reported negative particle charge [16], which resulted in a modified lymphatic targeting profile in these studies [13].

Plasma concentration levels above the 4× IC_{90} of 664 ng/mL denoted therapeutically relevant concentrations. A summary of the CAB C_{max} and T_{max} values obtained in plasma and tissue samples is given in Table S1.

After intramuscular injection of long-acting CAB nanosuspension at a dose of 5 mg/kg, therapeutically relevant plasma concentrations were reached after 4 h (7,367 ± 1318 ng/mL, n = 4). These were maintained throughout the course of the study. Maximum plasma levels of 44,555 ± 5877 ng/mL (C_{max}, n = 4) were reached after 5 d (T_{max}). The $AUC_{0–28}$ was 727,136 ng/mL*d. After 10 d (30,528 ± 840 ng/mL, n = 4), a drop in CAB plasma levels was observed. This decrease was significantly different ($p = 0.0003$) compared to 7 d (41,747 ± 1617 ng/mL, n = 4). However, the increase after 13 d (35,231 ± 3832 ng/mL, n = 4) was not significantly different ($p = 0.0564$) compared to 10 d. In the MAP cohort, therapeutically relevant plasma concentrations were also reached after 4 h (2,980 ± 1494 ng/mL, n = 4) and maintained throughout the course of the study. Maximum plasma levels of 29,413 ± 4434 ng/mL (C_{max}, n = 4) were only reached after 7 d (T_{max}). The $AUC_{0–28}$ was 275,998 ng/mL*d. After 5 d (16,009 ± 5723 ng/mL, n = 4), a drop in CAB plasma levels was observed. However, this decrease was not significantly different compared to the previous sample point (3 d, 28,890 ± 10,922 ng/mL, n = 4, $p = 0.0908$) or the following sample point (7 d, 29,413 ± 4434 ng/mL, n = 4, $p = 0.9947$). The in vivo plasma profiles are displayed in Fig. 8. The relative bioavailability for CAB-loaded MAPs was 51%.

Dissolving MAPs based on PVA-PVP were previously produced containing CAB, CAB-Na and CAB-NS, which are commercially available

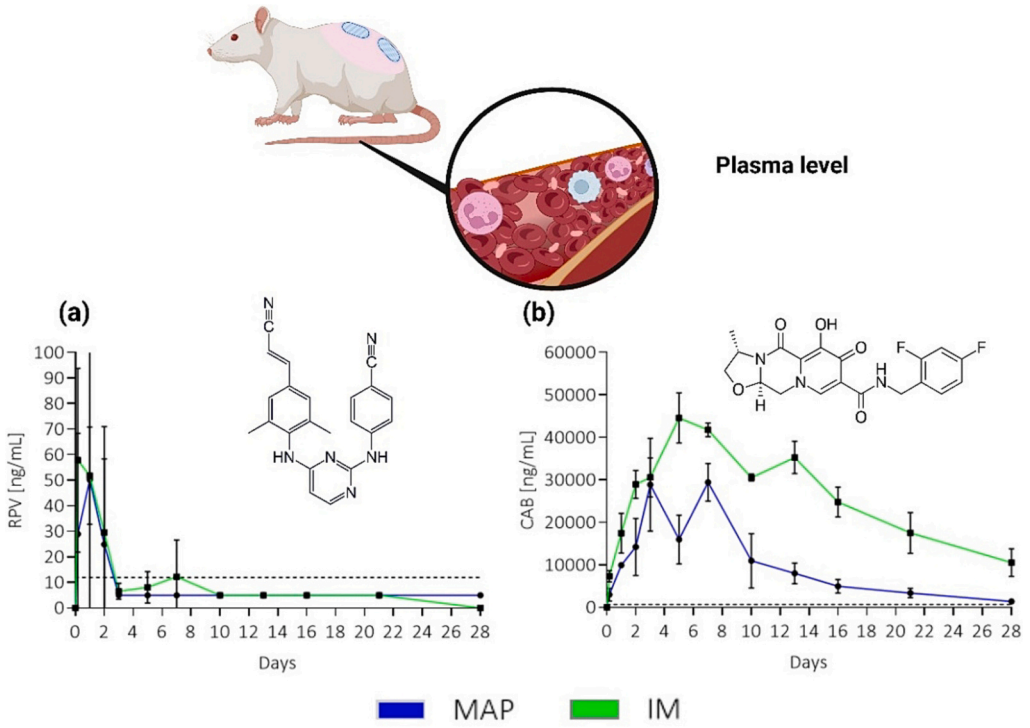

Fig. 8. (A) RPV and (B) CAB plasma levels [ng/mL] in female Sprague Dawley rats after intramuscular (IM) injection of 5 mg/kg RPV and 5 mg/kg CAB or application of two RPV-loaded (MAPs (means ± SD, $n = 4$). Therapeutically relevant concentrations are indicated by the dashed black line for RPV ($IC_{90} = 12$ ng/mL) and CAB ($IC_{90} = 166$ ng/mL).

[21]. In this work, the authors observed a higher C_{max} as well as a prolonged T_{max} for CAB-Na MAPs (C_{max} = 39.3 μg/mL/Tmax = 6 days) when compared with CAB MAPs (C_{max} = 18.7 $_{μg/mL/Tmax}$ = 6 days) or CAB-NS MAPs (C_{max} = 18.1 μg/mL/Tmax = 5 days). Volpe-Zanutto et al. [15] used a different approach to deliver CAB, in which they used hydrogel-forming MAPs based on PVA-PVP and citric acid crosslinked at 130 °C. The drug reservoir placed atop the hydrogel MAPs contained CAB-Na complexed with 2-hydroxypropyl-β-cyclodextrin. In this work, the authors were able to deliver higher therapeutic drug levels for up to 28 days, achieving a C_{max} of 58.98 ± 9.95 μg/mL and a T_{max} at 3 days, but with lower delivery efficiency due to the high amount of drug loaded in the reservoir. Moffatt et al. [16] applied two MAPs containing CAB nanosuspensions, and the authors were able to detect a C_{max} of 12 μg/mL (T_{max} = 9 days). In the present work, we also applied two CAB-loaded MAPs, obtaining a higher C_{max} of 29,413 ± 4434 ng/mL (T_{max} = 7 days) and, consequently, a higher relative bioavailability (51%) when compared with previously published work [15,16,21,44].

3.3.2.2. Lymph nodes. RPV and CAB concentrations in lymph nodes from three different sites were analyzed. When looking at axillary lymph nodes (Fig. 9 (a-d)) in the MAP cohort, 1, 3 and 7 d after application, therapeutically relevant but differing RPV concentrations ranging between 48 ng/g (7 d) and 2466 ng/g (3 d) were reached. After 10 d, therapeutically relevant concentrations were observed in only two animals. After 28 d, RPV was detectable in all animals but not quantifiable. Overall, concentrations varied considerably between different animals. For the intramuscular cohort, therapeutically relevant levels were only measured 1 d after injection (18 ± 2 ng/g, n = 4). On all other days, RPV was detectable but not quantifiable.

When looking at the uptake into iliac lymph nodes (Fig. 9 (b-e)) of the MAP cohort, therapeutically relevant concentrations were obtained 1 d after application (523 ± 171 ng/g, n = 4). After 3 d, only two animals had therapeutically relevant RPV levels; after 7 d, one animal and after 10 d, three animals. After 28 d, only traces of RPV were detected in all animals. In the intramuscular cohort, therapeutically relevant concentrations were detected up to 28 d after application in all but two animals (one animal 7 d and one 28 d after application). Concentrations reached 125,732 ng/g (3 d).

In external lumbar lymph nodes (Fig. 9 (c-f)) of the MAP cohort, therapeutically relevant concentrations were achieved in all animals 1, 3, 7 and 10 d after application (ranging from 88 ng/g to 5112 ng/g). Only one animal after 10 d showed just traces of RPV. After 28 d, RPV was detectable in all animals but not quantifiable. After intramuscular injection, only two animals showed high RPV concentrations after 1 d (45,453 ng/g and 2762 ng/g) and one animal after 10 d (53 ng/g). All other animals showed only traces of RPV that were not quantifiable. After 28 d, no RPV was detected in the external lumbar lymph nodes of the intramuscular cohort.

The %DTE and %DTP values for lymph-targeted RPV delivery via MAPs in comparison to intramuscular injections at individual sample points are displayed in Table 2. Values for 28 d were not assessed, as only drug traces could be detected. Delivery of RPV via MAPs to axillary and external lumbar lymph nodes was clearly superior compared to intramuscular injections, with %DTP values of 100% after 1, 3, and 7 d and 96% (axillary lymph nodes) or 92% (external lumbar lymph

Table 2
Percentage drug targeting efficiency (%DTE) and direct transport percentage (%DTP) for lymph-targeted delivery of RPV via MAPs compared to IM injections. The mean concentration levels (n = 4) on the respective study days were compared. %DTE > 100% shows superior lymph-targeted delivery via MAPs. %DTP values can vary from -∞ to 100%. Positive values show effective lymph-targeted delivery.

Day	Axillary lymph nodes		Iliac lymph nodes		External lumbar lymph nodes	
	%DTE	%DTP	%DTE	%DTP	%DTE	%DTP
1	83,562	100	2	−5314	103,144	100
3	83,797	100	0	−214,867	149,316	100
7	66,701	100	6	−1565	208,616	100
10	2719	96	7	−1359	1310	92

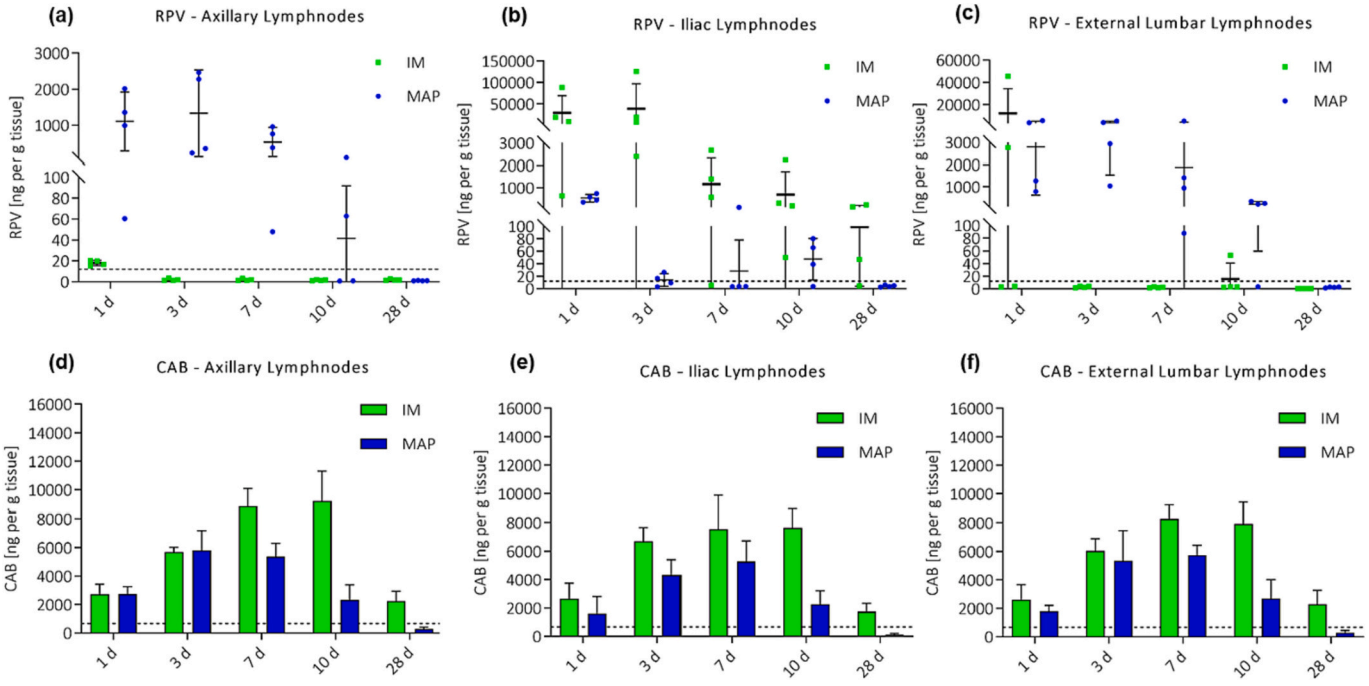

Fig. 9. (a) RPV and (b) CAB concentration levels [ng/g tissue] in axillary lymph nodes; (c) RPV and (d) CAB levels [ng/g tissue] in iliac lymph nodes; (e) RPV and (f) CAB levels [ng/g tissue] in external lumbar lymph nodes harvested from female Sprague Dawley rats after intramuscular (IM) injection of 5 mg/kg RPV or application of two RPV-MAPs (plotted are individual values and means ± SD, n = 4). Therapeutically relevant concentrations are indicated by the dashed black line for RPV (IC_{90} = 12 ng/mL) and CAB (IC_{90} = 166 ng/mL).

nodes) after 10 d. For iliac lymph nodes, the opposite effect was observed. Individual values were identified as outliers and excluded from calculations, that is, one concentration level achieved in axillary lymph nodes after MAP application (1 d, 60 ng/g, low in comparison to other values) and two values obtained from external lumbar lymph nodes after intramuscular injection (1 d, 45,453 ng/g and 2762 ng/g, high in comparison to other values).

Regarding CAB concentrations in the axillary lymph nodes (Fig. 9 (d)), maximum concentration levels of 9225 ± 2086 ng/g ($n = 4$) were reached 10 d after intramuscular injection of CAB. In the MAP cohort, maximum levels of 5808 ± 1360 ng/g (n = 4) were reached after 3 d. When comparing the concentration levels at each time point, there was no significant difference ($p > 0.5628$) after 1 d, 7 d and 10 d. After 3 d, the concentrations in axillary lymph nodes taken from the MAP cohort were significantly higher ($p = 0.0161$). After 28 d, however, they were significantly lower ($p = 0.0402$), and CAB levels in the MAP cohort fell below 664 ng/mL.

In iliac lymph nodes (Fig. 9 (e)) excised from the intramuscular cohort, maximum concentration levels of 7636 ± 1311 ng/g ($n = 4$) were reached 10 d after application. In the MAP cohort, maximum concentration levels of 5280 ± 1433 ng/g (n = 4) were reached 7 d after application. When comparing the dose-adjusted concentration levels, no significant difference was observed up to 10 d ($p > 0.4742$). After 28 d, however, CAB levels in the MAP cohort fell below 664 ng/mL and were significantly lower ($p = 0.0203$) than those in the intramuscular cohort.

In external lumbar lymph nodes (Fig. 9 (f)) excised from the intramuscular cohort, maximum concentration levels of 8282 ± 926 ng/g (n = 4) were reached 7 d after administration. In the MAP cohort, maximum concentration levels of 7726 ± 711 ng/g (n = 4) were also reached 7 d after application. When comparing the dose-adjusted concentration levels, no significant difference was observed up to 10 d ($p > 0.0719$). After 28 d, however, CAB levels in the MAP cohort fell below 664 ng/mL and were significantly lower ($p = 0.0259$) than those in the intramuscular cohort.

The %DTE and %DTP values for lymph-targeted CAB delivery via MAPs in comparison to intramuscular injections at individual sample points are displayed in Table 3. After 1 d, MAPs showed superior lymph-targeted delivery of CAB with %DTE values of 177%, 108%, and 120% for axillary, iliac, and external lumbar lymph nodes, respectively. After 3 d, only uptake into axillary lymph nodes was superior for MAPs, with a %DTE of 108%. On the following days, the DTE was equal to or less efficient for MAPs.

3.3.2.3. Vaginal tissues. In vaginal tissues, therapeutically relevant RPV levels (Fig. 10 (a)) were detected in three of four animals in the MAP cohort (18 ng/g, 64 ng/g, 193 ng/g) but only in one animal of the intramuscular cohort (48 ng/g) after 1 d. After 3 d, only traces of RPV were detected. After 7 d, one animal in each cohort showed therapeutically relevant RPV levels (intramuscular 356 ng/g, MAP 16 ng/g). In the MAP cohort, RPV traces could be detected up to 28 d after application. After intramuscular injection, RPV was still traceable after 10 d but not after 28 d.

CAB concentrations in vaginal tissue (Fig. 10 (b)) were detected in female rats after an intramuscular injection of CAB, reaching maximum concentrations of 11,481 ± 3316 ng/g ($n = 4$) after 7 d. In the MAP cohort, maximum levels of 8218 ± 2795 ng/g (n = 4) were reached after 3 d. At this time point, dose-adjusted concentrations in the MAP cohort were significantly higher ($p = 0.0201$) than in the intramuscular cohort. On the other days, there was no significant difference ($p > 0.1507$). After 28 d, CAB levels were not therapeutically relevant in three out of four animals of the MAP cohort.

3.3.2.4. Livers. In livers (Fig. 10 (c)), therapeutically relevant RPV concentrations were observed in individual animals of both cohorts up to 28 d after either intramuscular injection of RPV or MAP application. Again, the results differed greatly between animals. The maximum values detected were 112 ng/g (intramuscular, 3 d) and 267 ng/g (MAP, 1 d).

For CAB, (Fig. 10 (d)), maximum concentrations of 6040 ± 1367 ng/g ($n = 4$) were reached 7 d after CAB intramuscular injection. In the MAP cohort, maximum levels of 4541 ± 1702 ng/g (n = 4) were reached after 7 d. When comparing the dose-adjusted concentrations, no significant difference was observed between the two cohorts at any sampling point ($p > 0.0924$). However, levels in the MAP cohort were not therapeutically relevant after 28 d.

3.3.2.5. Kidneys. In kidneys (Fig. 10 (e)), therapeutically relevant levels of RPV were obtained in all animals of both cohorts 1 d after application, in the MAP cohort up to 7 d after application and in the intramuscular cohort up to 3 d after application. After 1 d, the variation in the intramuscular cohort was small (112 ± 10 ng/g, n = 4), whereas the results differed more for the MAP cohort (ranging from 34 ng/g to 293 ng/g).

Regarding CAB concentrations in kidneys (Fig. 10 (f)), maximum concentrations of 11,377 ± 2177 ng/g ($n = 4$) were reached 7 d after a CAB intramuscular injection. In the MAP cohort, maximum levels of 9000 ± 1259 ng/g (n = 4) were reached after 7 d. When comparing the dose-adjusted concentrations, no significant difference was observed between the two cohorts up to 10 d after application ($p > 0.0979$). After 28 d, CAB levels were significantly higher in the kidneys of the intramuscular cohort ($p = 0.0007$). In the MAP cohort, values dropped below therapeutically relevant levels.

3.3.2.6. Spleens. In spleens (Fig. 10 (g)), RPV concentrations were below the limit of quantification in nearly all animals. Only after 1 d, three out of four animals in the MAP cohort have therapeutically relevant levels (ranging from 21 ng/g to 132 ng/g). On the following days, only traces of RPV could be detected in all animals. After intramuscular injection of RPV, no therapeutically relevant RPV levels were detected in the animals.

For CAB (Fig. 10 (h)), maximum concentrations of 4013 ± 319 ng/g (n = 4) were reached in spleens 7 d after a CAB intramuscular injection was administered. In the MAP cohort, maximum levels of 2513 ± 395 ng/g (n = 4) were reached after 7 d. When comparing the dose-adjusted concentrations, no significant difference was observed between the two cohorts up to 10 d after application ($p > 0.0895$). After 28 d, CAB levels were significantly higher in spleens of the intramuscular cohort ($p = 0.0011$). They dropped below therapeutically relevant levels in all animals of the MAP cohort and in two animals of the intramuscular cohort.

3.3.2.7. Skin. Analysis of abdominal skin samples (Fig. 10 (i)) showed therapeutically relevant RPV concentrations in two animals of the intramuscular cohort 1 d after injection (14 ng/g and 32 ng/g). RPV traces could be detected up to 10 d after application. In the MAP cohort, values ranging from 103 ng/g to 263 ng/g were detected 1 d after

Table 3
Percentage drug targeting efficiency (%DTE) and direct transport percentage (% DTP) for lymph-targeted delivery of CAB via MAPs compared to IM injections. The mean concentration levels ($n = 4$) on the respective study days were compared. %DTE > 100% shows superior lymph-targeted delivery via MAPs. % DTP values can vary from -∞ to 100%. Positive values show effective lymph-targeted delivery.

Day	Axillary lymph nodes		Iliac lymph nodes		External lumbar lymph nodes	
	%DTE	%DTP	%DTE	%DTP	%DTE	%DTP
1	177	43	108	7	120	17
3	108	8	68	−46	94	−7
7	86	−16	99	−1	98	−2
10	71	−41	82	−21	94	−6
28	100	0	57	−74	100	0

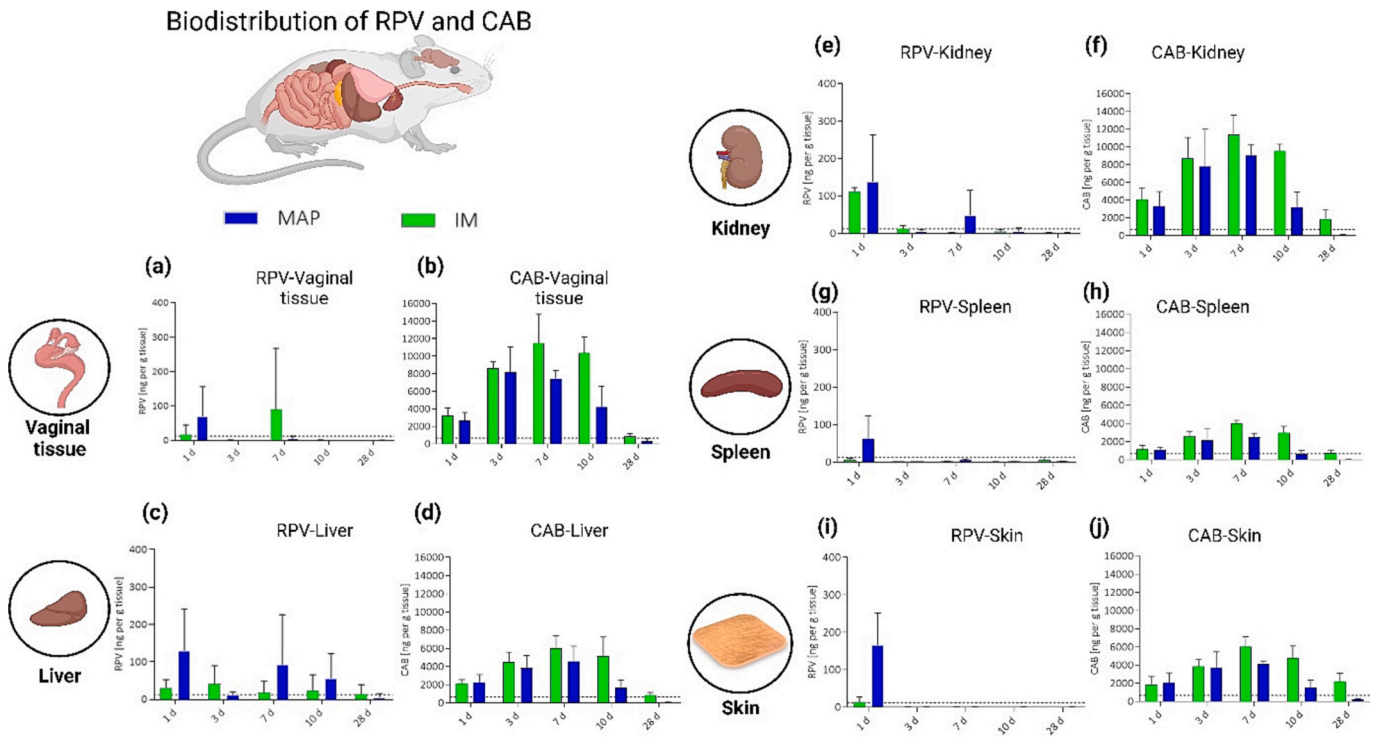

Fig. 10. (a) RPV and (b) CAB vaginal tissues [ng/g tissue]; (c) RPV and (d) CAB levels [ng/g tissue] in livers; (e) RPV and (f) CAB concentrations [ng/g tissue] in kidneys; (g) RPV and (h) CAB levels [ng/g tissue] in spleens and (i) RPV and (j) in the skin [expressed in ng/g tissue] from female Sprague Dawley rats after intramuscular (IM) injection of 5 mg/kg in female Sprague Dawley rats after intramuscular (IM) injection of 5 mg/kg CAB or application of two CAB-loaded MAPs (means ± SD, $n = 4$). Therapeutically relevant concentrations are indicated by the dashed black line RPV ($IC_{90} = 12$ ng/mL), and CAB ($IC_{90} = 166$ ng/mL).

application. One value was excluded due to suspected contamination with RPV from the application site. On all following days (up to 28 d), only RPV traces were detected.

Regarding the results of CAB deposition in animal-harvested abdominal skin (Fig. 10 (j)) after intramuscular injection of CAB, maximum concentrations of 6055 ± 1055 ng/g (n = 4) were reached after 7 d. In the MAP cohort, maximum levels of 4131 ± 303 ng/g (n = 4) were reached after 7 d. When comparing the dose-adjusted concentrations, no significant difference was observed between the two cohorts up to 10 d after application ($p > 0.0924$). After 28 d, CAB levels were significantly higher in the skin of the intramuscular cohort ($p = 0.0122$). They dropped below therapeutically relevant levels in all animals of the MAP cohort.

Lymph-targeted delivery of antiretroviral agents is highly desirable, and suppression of viral reservoirs in the lymphatic system could be a major milestone in the ongoing fight against HIV. Current HAART options successfully control viral replication in the systemic circulation; however, upon therapy interruption, rebound viraemia can occur because antiretroviral drugs from present delivery platforms permeate poorly into lymphoid tissues. Previous approaches for improved lymphatic uptake focused on the subcutaneous injection of lipid-associated nanoparticulate systems [45] or the oral administration of lipophilic ester prodrugs [46]. This work aimed for the first time at passive lymph-targeted delivery of two antiretroviral agents through formulation as NCs and intradermal application by dissolving polymeric MAPs. Although one previous study showed that MAPs might improve the lymphatic uptake of RPV [35], no study has yet been conducted that focused on the lymphatic delivery of RPV and CAB via MAPs. A combined pharmacokinetics and full biodistribution study (by dissection) was conducted in female Sprague Dawley rats to investigate the simultaneous delivery and biodistribution of RPV and CAB NCs via MAPs compared to intramuscular injections of commercially available prolonged-release nanosuspensions. The developed multilayered MAPs were extensively characterized in vitro and ex vivo (item 3.2.) prior to in vivo application.

Two RPV-loaded and two CAB-loaded MAPs were applied to the back of each animal for 24 h. As expected from preceding ex vivo studies, MAPs inserted fully into the skin of the animals and deposited their drug intradermally. The novel multilayered design enabled full MN separation, and only minimal polymer residues were visible on the skin. Any remains could be easily removed with a wet paper towel. This is of high importance considering the user friendliness and acceptability of future products. Short application times are another important factor to be considered when translating developed products to possible use in humans. Due to animal welfare restrictions, MAPs had to be kept in place for 24 h during the in vivo study.

After removal of MAPs, deposited drug could be clearly seen in the skin. After 1 d, 215 ± 82 μg RPV ($n = 8$) was deposited in the skin. Compared to ex vivo skin deposition studies in neonatal porcine skin (366 ± 139 μg, $n = 6$), there was no significant difference ($p = 0.2008$). This shows that the results obtained in the employed ex vivo model can be translated to in vivo studies. Furthermore, it can be concluded that the amount of drug deposited ex vivo after 24 h is comparable to the dose available for in vivo delivery. For CAB, the amount of drug detected in in vivo application site samples was significantly lower ($p = 0.0244$) than in ex vivo experiments (123 ± 54 μg ($n = 8$) compared to 463 ± 143 μg ($n = 6$)). CAB is less hydrophobic than RPV, and when looking at plasma and different tissue samples, high CAB levels (9958 ± 535 ng/mL) were achieved after 24 h and maintained over several days. This shows the fast absorption and distribution of CAB in comparison to RPV and is a possible explanation for the low amounts of CAB detected at application sites after 24 h. After 10 d, 53 ± 44 μg ($n = 8$) could still be detected in RPV application sites (no RPV detectable in abdominal skin samples), whereas for CAB, no significant difference ($p = 0.7457$) was seen compared to skin taken from the abdomen of the animals.

RPV exhibited low plasma concentrations (below the limit of quantification from 3 d onward in both cohorts), which can be partly accounted for by the considerable hydrophobicity of the drug and the

slow and prolonged release from application sites. Hydrophobicity of the delivered system along with surface charge facilitate a higher lymphatic uptake by directly influencing the process of phagocytosis by attracting opsonins on the hydrophobic surface [47,48]. For the same reason, the results obtained for plasma and tissue samples showed high variation between animals. Maximum plasma concentrations of 58 ± 36 ng/mL (n = 4) were obtained 4 h after intramuscular injection and maintained over 1 d. In the MAP cohort, two animals had therapeutically relevant plasma levels (rat 1: 87 ng/mL; rat 4: 19 ng/mL) after 4 h and one animal after 1 d (186 ng/mL). While RPV could be detected in the MAP cohort until the end of the study, no drug was detectable in the plasma 28 d after intramuscular injection. This indicated that intradermal application via MAPs prolonged the release of RPV.

Interestingly, in contrast to the low RPV levels achieved in plasma, high concentration levels were detected in the lymph nodes, especially after MAP application as intended. Lymph nodes from three different sites were harvested and analyzed. In axillary lymph nodes, which drain from the skin and underlying musculature [35], therapeutically relevant concentrations were only measured 1 d after intramuscular injection (18 ± 2 ng/g, n = 4). However, in the MAP cohort, 1, 3 and 7 d after application, RPV concentrations ranging between 48 ng/g (7 d) and 2466 ng/g (3 d) were reached in all animals, and even after 10 d, therapeutically relevant concentrations were observed in two animals. %DTP to the lymph nodes was 100% up to 7 d and 96% after 10 d. This shows that the combination of lower dose and smaller particle size of RPV NCs with MAPs led to direct uptake into the lymph from the skin application site and that NCs were retained in lymph nodes over several days, resulting in less drug in plasma due to the localized drug reservoir in the lymph nodes. Similar results were obtained for external lumbar lymph nodes, which drain from abdominal, pelvic and thoracic organs [35] and are located close to the application sites, with concentrations of up to 5112 ng/g achieved in the MAP cohort and a %DTP of 100% up to 7 d and 92% after 10 d. Only traces of RPV were detected in most animals after intramuscular injection. However, two animals showed considerably high RPV concentrations after 1 d (45,453 ng/g and 2762 ng/g) and one animal after 10 d (53 ng/g). A possible explanation for such high values in individual animals compared to other animals of the same group might be that during intramuscular injection, lymph vessels were hit in individual animals, and some RPV NCs were injected directly into the lymph. These then remained in lymph nodes due to their high hydrophobicity. Contrary to the other examined lymph nodes, iliac lymph nodes drain from organs in the caudal abdomen and pelvis, including the urogenital tract and, most importantly, the pelvic limbs [49], that is, the hind legs of rats. This explains why RPV levels of up to 125,732 ng/g (3 d) were detected in iliac lymph nodes after intramuscular injection (applied to the hind legs). Therapeutically relevant concentrations were detected up to 28 d after application. In contrast, in the MAP cohort, therapeutically relevant levels of 523 ± 171 ng/g (n = 4) were detected only in all animals after 1 d. After 3 d, only two animals had therapeutically relevant RPV levels, one animal after 7 d and three animals after 10 d. After 28 d, only traces of RPV were detected in all animals.

In addition to lymph nodes, vaginal tissues were excised from the treated animals as one of the main transmission sites of HIV. Therapeutically relevant RPV levels were detected in three out of four animals of the MAP cohort but only in one animal of the intramuscular cohort after 1 d. Only in the MAP cohort was RPV still traceable after 28 d, indicating that application of MAPs might have a positive effect on RPV levels in vaginal tissues and, thus, might decrease the risk of transmission. Antiretroviral therapy is often associated with liver toxicity caused by elevations in transaminases, most common in individuals with chronic hepatitis C and B [50]. RPV is mainly metabolized by CYP3A4 in the liver [51]. RPV levels detected in livers were slightly increased after MAP application with maximum values of up to 267 ng/g (MAP, 1 d) compared to up to 112 ng/g (intramuscular, 3 d). However, hepatotoxicity caused by RPV is rare [52]; thus, slightly elevated RPV levels might not greatly affect the rate of serum aminotransferases. More extensive studies will be necessary to evaluate the significance of observed differences and to study possible toxic effects. Renal elimination of RPV is negligible [51]. Renal RPV levels in the MAP cohort were slightly elevated after 1 d and 7 d in individual animals (up to 293 ng/g) compared to intramuscular application (112 ± 10 ng/g, n = 4, 1 d). On all other days, renal levels were minimal. The spleen is one of the organs of the lymphatic system but has only efferent lymph vessels and is, therefore, supplied through the general cardiovascular circulation. RPV concentrations were below the limit of quantification in the spleens of all but individual animals. While in the MAP cohort three out of four animals had therapeutically relevant levels (ranging from 21 ng/g to 132 ng/g) after 1 d, no therapeutically relevant levels were detected in any animal in the intramuscular cohort. Traces of RPV could be detected in the abdominal skin of animals of both cohorts. Only in the MAP cohort were concentrations of up to 263 ng/g detected after 1 d. However, it is suspected that these were obtained due to contamination with RPV from application sites.

Contrary to RPV, CAB concentration levels in plasma and across all organs were more consistent (less variation between animals) due to better delivery efficiency. CAB showed high biodistribution across analyzed tissues. For statistical comparison of the two cohorts, CAB tissue levels were adjusted for dose differences of 5 mg/kg for intramuscular injection and 3.68 mg/kg for MAP application (factor 1.4). In the intramuscular cohort, maximum plasma levels of 44,555 ± 5877 ng/mL (C_{max}, n = 4) were reached after 5 d (T_{max}). The $AUC_{0–28}$ was 727,136 ng/mL*d. In the MAP cohort, maximum plasma levels of 29,413 ± 4434 ng/mL (C_{max}, n = 4) were only reached after 7 d (T_{max}). The $AUC_{0–28}$ was 275,998 ng/mL*d. The relative bioavailability for CAB-loaded MAPs was 51%. In both cohorts, therapeutically relevant concentrations were reached after 4 h and maintained throughout the course of the study. In both cohorts, a drop in CAB plasma levels was observed. A possible explanation might be that long-acting CAB exhibits absorption-limited (flip-flop) kinetics [53]. It is, however, more likely that this statistically no significant drop was experienced due to sampling of animals from different application groups. CAB tissue level profiles followed plasma profiles very closely, and therapeutic levels were maintained in all analyzed tissues up to 10 d after application and in most cases until the end of the study. In contrast to RPV, renal CAB levels were higher than hepatic levels, as CAB is predominantly metabolized in the kidneys (UGT1A1) [53]. In general, when comparing dose-adjusted concentration levels, only slight differences were observed between the MAP cohort and the intramuscular cohort, as shown in detail in the results section. This indicates that dissolving MAPs could be a feasible alternative in the delivery of long-acting CAB.

Regarding the lymph-targeted delivery of antiretrovirals, when looking at.%DTE and %DTP values, MAPs were less superior for lymph uptake of CAB than it was observed for RPV. Nevertheless, after 1 d, MAPs showed superior lymph-targeted delivery of CAB with %DTE values of 177%, 108% and 120% for axillary, iliac and external lumbar lymph nodes, respectively. After 3 d, only uptake into axillary lymph nodes was superior for MAPs compared to intramuscular injection, with a %DTE of 108%. Furthermore, maximum concentration levels in lymph nodes were reached either earlier (axillary lymph nodes, 3 d) or on the same day as in plasma (7 d) in the MAP cohort. In contrast, times of maximum concentrations in the lymph nodes were delayed in the intramuscular cohort compared with plasma (7 or 10 d compared with 5 d). These results indicate that even though lymph concentration levels in both cohorts were high, CAB might have been taken up by lymph immediately from the interstitium after MAP application, whereas after intramuscular application, CAB was possibly distributed from plasma into lymph and then retained in lymph nodes.

In this study, RPV- and CAB-loaded MAPs were compared to intramuscular application of the same drugs. It should be noted that even though RPV and CAB are given as prolonged release nanosuspensions for injection, this is a highly novel therapeutic approach, and the majority

of HIV-infected individuals are treated orally with a combination of antiretrovirals. After oral application of antiretrovirals, drug levels detected in the lymphatic system are generally low [46]. Even the intramuscular or subcutaneous injection of solubilized antiretrovirals already increases lymphatic uptake compared to oral administration, as shown in a recently published study [54]. If the lymphatic uptake after MAP application was to be compared to an oral control group, an even higher advantage of MAPs might be expected.

Comparison between the lymph-targeted uptake of RPV and CAB shows that not only the formulation approach but also the drug characteristics play an important role in the biodistribution of therapeutic agents. Both drugs are practically insoluble in aqueous media and are classified as Class II (high permeability, low solubility) in the Biopharmaceutics Classification System (BCS). However, the logP value of RPV is >4.16 [55], while it is set at 0.16 for CAB [56]. Both drugs were formulated as NCs of approximately the same size with the same matrix used for fabrication of dissolving MAPs. From the results, it can be suspected that RPV might stay in its nanocrystalline form over an extended period upon application. The NCs diffuse through the interstitium into lymph vessels and accumulate in lymph nodes, where they remain while slow dissolution occurs. For CAB, on the contrary, a certain proportion of NCs might possibly travel to the lymph immediately upon application, explaining the higher results on the first days after MAP application. However, it seems that a large proportion of administered CAB NCs dissolve and might, thus, be taken up by blood capillaries from where CAB is distributed throughout body tissues. Furthermore, the obtained results indicate that CAB is not retained in lymph nodes for an extended period.

MAPs have shown promise for the delivery of ARV drugs and could bring significant benefit to users [57]. This study showed that therapeutically relevant drug levels could be achieved in the plasma and tissues of rats after application of RPV- and CAB-loaded MAPs. Extrapolating doses required in humans from rat models requires thorough considerations, as pharmacokinetics in rats and humans are different. However, taking into consideration the estimated amount of drug delivered per area of MAP, careful approximations can be made regarding the MAP size required to deliver doses required in humans [58]. To date, MAPs loaded with RPV or CAB have never been tested in humans, but a physiologically based pharmacokinetic model for the simulation of human pharmacokinetics of RPV- or CAB-loaded MAPs was recently developed [59]. This model estimated the optimal dose required in a four-weekly dosing regimen to achieve therapeutically relevant plasma levels. Calculations indicated that after an initial loading dose of 360 mg for CAB and 1080 mg for RPV, maintenance doses of 180 mg and 540 mg, respectively, applied every four weeks were required to maintain target concentrations comparable to intramuscular injection of 400 mg CAB or 600 mg RPV [59]. The doses deposited in skin after MAP application for 24 h obtained ex vivo were 0.366 mg for RPV and 0.463 mg for CAB, using an MAP size of 0.75 cm^2. Furthermore, it is important to note that the aim of this study was not to deliver drugs for therapeutically relevant plasma levels but rather for viral suppression in the lymphatic system. This in vivo study showed that it was possible to deliver therapeutically relevant concentrations of RPV and CAB to the lymph nodes using the developed combination of NCs and multilayered MAPs. Future studies could be aimed at the formulation of MAPs with increased delivery efficiency for reduced patch sizes and dosing frequencies. Furthermore, the development of cocrystals of RPV and CAB for enhanced lymphatic uptake of CAB, as mentioned above, could be explored. The effect of elevated drug concentration levels in lymph nodes after intradermal application via MAPs on the suppression of viral reservoirs will then need to be studied in suitable infection models.

4. Conclusions

This study has shown, for the first time, the successful delivery of RPV and CAB NCs to the lymphatic system of a suitable in vivo model in a targeted manner using dissolving polymeric MAPs. The antiretrovirals were visibly deposited in the skin after an application time of 24 h. Analysis of plasma and various tissue samples showed extensive distribution of both drugs throughout the body, with therapeutically relevant concentrations levels reached CAB-loaded MAPs presented superior initial lymphatic uptake compared to intramuscular injection of a commercially available prolonged-release nanosuspension. In addition to being a user-friendly alternative to intramuscular injections, the developed MAPs have the potential to target viral reservoirs in the lymph that cannot be accessed through currently available common treatment options.

CRediT authorship contribution statement

Inken K. Ramöller: Validation, Project administration, Methodology, Investigation, Formal analysis, Data curation, Conceptualization. **Fabiana Volpe-Zanutto:** Writing – review & editing, Writing – original draft, Formal analysis, Data curation, Conceptualization. **Lalitkumar K. Vora:** Writing – review & editing, Visualization, Supervision, Methodology, Investigation, Formal analysis. **Marco T.A. Abbate:** Validation, Methodology, Investigation, Formal analysis, Data curation. **Aaron R.J. Hutton:** Methodology, Investigation. **Peter E. McKenna:** Writing – review & editing, Writing – original draft, Methodology, Investigation. **Ke Peng:** Methodology, Investigation. **Ismaiel A. Tekko:** Methodology, Investigation. **Akmal Sabri:** Software, Methodology. **Emma McAlister:** Methodology. **Helen O. McCarthy:** Supervision, Resources. **Alejandro J. Paredes:** Writing – review & editing, Writing – original draft, Supervision, Investigation, Formal analysis, Data curation. **Ryan F. Donnelly:** Writing – review & editing, Writing – original draft, Visualization, Supervision, Conceptualization.

Data availability

Data will be made available on request.

Acknowledgements

The authors would like to thank ViiV Healthcare Ltd. and Janssen Pharmaceutica for providing the nanosuspension formulations and bulk powder drugs of CAB and RPV, respectively. This project was also supported in part by EPSRC grant EP/S028919/1 and MAPs for Peds: Development of a Microarray Patch for Delivery of Long-Acting Antiretrovirals for Treatment of Pediatric HIV Infection was funded by the Eunice Kennedy Shriver National Institute of Child Health & Human Development and the National Institute of Allergy and Infectious Diseases (NIAID) under NIAID grant number 1R61AI149642-01.

Appendix A. Supplementary data

Supplementary data to this article can be found online at https://doi.org/10.1016/j.jconrel.2024.01.010.

References

[1] World Health Organization, Fact Sheet HIV/AIDS, Geneva, 2020.
[2] R.N.O. Cobucci, P.H. Lima, P.C. de Souza, V.V. Costa, M. Cornetta, J.V. Fernandes, A.K. Gonçalves, Assessing the impact of HAART on the incidence of defining and non-defining AIDS cancers among patients with HIV/AIDS: a systematic review, J. Infect. Public Health 8 (2015) 1–10, https://doi.org/10.1016/j.jiph.2014.08.003.
[3] World Health Organization, Consolidated Guidelines on the Use of Antiretroviral Drugs for Treating and Preventing HIV Infection: Recommendations for a Public Health Approach, 2nd ed., 2016. Geneva.
[4] M. Barnhart, Long-acting HIV treatment and prevention: closer to the threshold, Glob. Heal. Sci. Pract. 5 (2017) 182–187, https://doi.org/10.9745/GHSP-D-17-00206.
[5] European mMedicines aAgency CHMP, Assessment report - Vocabria - Procedure No. EMEA/H/C/004976/0000, 2020.

[6] S. Swindells, J.-F. Andrade-Villanueva, G.J. Richmond, G. Rizzardini, A. Baumgarten, M. Masiá, G. Latiff, V. Pokrovsky, F. Bredeek, G. Smith, P. Cahn, Y.-S. Kim, S.L. Ford, C.L. Talarico, P. Patel, V. Chounta, H. Crauwels, W. Parys, S. Vanveggel, J. Mrus, J. Huang, C.M. Harrington, K.J. Hudson, D.A. Margolis, K. Y. Smith, P.E. Williams, W.R. Spreen, Long-acting cabotegravir and rilpivirine for maintenance of HIV-1 suppression, N. Engl. J. Med. 382 (2020) 1112–1123, https://doi.org/10.1056/nejmoa1904398.

[7] A.J. Paredes, P.E. McKenna, I.K. Ramöller, Y.A. Naser, F. Volpe-Zanutto, M. Li, M. T.A. Abbate, L. Zhao, C. Zhang, J.M. Abu-Ershaid, X. Dai, R.F. Donnelly, Microarray patches: poking a hole in the challenges faced when delivering poorly soluble drugs, Adv. Funct. Mater. 2005792 (2020) 1–27, https://doi.org/10.1002/adfm.202005792.

[8] N.L. Trevaskis, L.M. Kaminskas, C.J.H. Porter, From sewer to saviour-targeting the lymphatic system to promote drug exposure and activity, Nat. Rev. Drug Discov. 14 (2015) 781–803, https://doi.org/10.1038/nrd4608.

[9] A.J. Harvey, S.A. Kaestner, D.E. Sutter, N.G. Harvey, J.A. Mikszta, R.J. Pettis, Microneedle-based intradermal delivery enables rapid lymphatic uptake and distribution of protein drugs, Pharm. Res. 28 (2011) 107–116, https://doi.org/10.1007/s11095-010-0123-9.

[10] A.D. Permana, I.A. Tekko, M.T.C. McCrudden, Q.K. Anjani, D. Ramadon, H. O. McCarthy, R.F. Donnelly, Solid lipid nanoparticle-based dissolving microneedles: a promising intradermal lymph targeting drug delivery system with potential for enhanced treatment of lymphatic filariasis, J. Control. Release 316 (2019) 34–52, https://doi.org/10.1016/j.jconrel.2019.10.004.

[11] E. Ramadan, T. Borg, G.M. Abdelghani, N.M. Saleh, Transdermal microneedle-mediated delivery of polymeric lamivudine-loaded nanoparticles, J. Pharm. Technol. Drug Res. 5 (2016) 1, https://doi.org/10.7243/2050-120x-5-1.

[12] M.T.C. Mc Crudden, E. Larrañeta, A. Clark, C. Jarrahian, A. Rein-Weston, S. Lachau-Durand, N. Niemeijer, P. Williams, C. Haeck, H.O. McCarthy, D. Zehrung, R.F. Donnelly, Design, formulation and evaluation of novel dissolving microarray patches containing a long-acting rilpivirine nanosuspension, J. Control. Release 292 (2018) 119–129, https://doi.org/10.1016/j.jconrel.2018.11.002.

[13] M.T.C. Mc Crudden, E. Larrañeta, A. Clark, C. Jarrahian, A. Rein-Weston, B. Creelman, Y. Moyo, S. Lachau-Durand, N. Niemeijer, P. Williams, H. O. McCarthy, D. Zehrung, R.F. Donnelly, Design, formulation, and evaluation of novel dissolving microarray patches containing rilpivirine for intravaginal delivery, Adv. Healthc. Mater. 8 (2019), https://doi.org/10.1002/adhm.201801510.

[14] I. Tekko, L. Vora, M. McCrudden, C. Jarrahian, A. Rein-Weston, D. Zehrung, P. Giffen, H. McCarthy, R. Donnelly, Novel dissolving bilayer microarray patches as a minimally invasive, efficient intradermal delivery system for a long-acting cabotegravir nanosuspension, In: 2019 Control. Release Soc. Annu. Meet. Expo., Valencia, Spain, 2019.

[15] F. Volpe-Zanutto, L.K. Vora, I.A. Tekko, P.E. McKenna, A.D. Permana, A.H. Sabri, Q.K. Anjani, H.O. McCarthy, A.J. Paredes, R.F. Donnelly, Hydrogel-forming microarray patches with cyclodextrin drug reservoirs for long-acting delivery of poorly soluble cabotegravir sodium for HIV pre-exposure prophylaxis, J. Control. Release 348 (2022) 771–785, https://doi.org/10.1016/j.jconrel.2022.06.028.

[16] K. Moffatt, I.A. Tekko, L. Vora, F. Volpe-Zanutto, A.R.J. Hutton, J. Mistilis, C. Jarrahian, N. Akhavein, A.D. Weber, H.O. McCarthy, R.F. Donnelly, Development and evaluation of dissolving microarray patches for co-administered and repeated intradermal delivery of long-acting Rilpivirine and Cabotegravir Nanosuspensions for Paediatric HIV antiretroviral therapy, Pharm. Res. (2022), https://doi.org/10.1007/s11095-022-03408-6.

[17] A.A. Khan, J. Mudassir, N. Mohtar, Y. Darwis, Advanced drug delivery to the lymphatic system: lipid-based nanoformulations, Int. J. Nanomedicine 8 (2013) 2733–2744, https://doi.org/10.2147/IJN.S41521.

[18] R. Müller, Junghanns, nanocrystal technology, drug delivery and clinical applications, Int. J. Nanomedicine 3 (2008) 295, https://doi.org/10.2147/ijn.s595.

[19] R.H. Müller, S. Gohla, C.M. Keck, State of the art of nanocrystals – special features, production, nanotoxicology aspects and intracellular delivery, Eur. J. Pharm. Biopharm. 78 (2011) 1–9. https://doi.org/10.1016/j.ejpb.2011.01.007.

[20] M.R. Gigliobianco, C. Casadidio, R. Censi, P. Di Martino, Nanocrystals of poorly soluble drugs: drug bioavailability and physicochemical stability, Pharmaceutics 10 (2018) 134, https://doi.org/10.3390/pharmaceutics10030134.

[21] I.A. Tekko, L.K. Vora, F. Volpe-Zanutto, K. Moffatt, C. Jarrahian, H.O. McCarthy, R. F. Donnelly, Novel bilayer microarray patch-assisted long-acting Micro-depot Cabotegravir intradermal delivery for HIV pre-exposure prophylaxis, Adv. Funct. Mater. (2021) 2106999, https://doi.org/10.1002/adfm.202106999.

[22] A.D. Permana, A.J. Paredes, F.V. Zanutto, M.N. Amir, I. Ismail, M.A. Bahar, S. D. Sumarheni, R.F. Donnelly Palma, Albendazole nanocrystal-based dissolving microneedles with improved pharmacokinetic performance for enhanced treatment of cystic echinococcosis, ACS Appl. Mater. Interfaces 13 (2021) 38745–38760, https://doi.org/10.1021/acsami.1c11179.

[23] F. Volpe-Zanutto, L. Tiburcio, A. Dian, M. Kirkby, A.J. Paredes, L.K. Vora, A. P. Bonfanti, I. Charlie-silva, C. Raposo, M.C. Figueiredo, I.M.O. Sousa, A. Brisibe, R. F. Donnelly, M. Ann, F. Trindade, Artemether and lumefantrine dissolving microneedle patches with improved pharmacokinetic performance and antimalarial efficacy in mice infected with Plasmodium yoelii 333 (2021) 298–315, https://doi.org/10.1016/j.jconrel.2021.03.036.

[24] I.K. Ramöller, E. McAlister, A. Bogan, A.S. Cordeiro, R.F. Donnelly, Novel design approaches in the fabrication of polymeric microarray patches via micromoulding, Micromachines. 11 (2020) 1–12, https://doi.org/10.3390/MI11060554.

[25] I.K. Ramöller, I.A. Tekko, H.O. McCarthy, R.F. Donnelly, Rapidly dissolving bilayer microneedle arrays – a minimally invasive transdermal drug delivery system for vitamin B12, Int. J. Pharm. 566 (2019) 299–306, https://doi.org/10.1016/J.IJPHARM.2019.05.066.

[26] A.D. Permana, A.J. Paredes, F. Volpe-Zanutto, Q.K. Anjani, E. Utomo, R. F. Donnelly, Dissolving microneedle-mediated dermal delivery of itraconazole nanocrystals for improved treatment of cutaneous candidiasis, Eur. J. Pharm. Biopharm. 154 (2020) 50–61, https://doi.org/10.1016/j.ejpb.2020.06.025.

[27] Q. Kurnia, F. Volpe-zanutto, K. Abdul, J. Calit, A. Hidayat, B. Sabri, N. Moreno-castellano, X.A. Gait, D.Y. Bargieri, R.F. Donnelly, Primaquine and chloroquine nano-sized solid dispersion-loaded dissolving microarray patches for the improved treatment of malaria caused by Plasmodium vivax 361 (2023) 385–401, https://doi.org/10.1016/j.jconrel.2023.08.009.

[28] J.M. Abu Ershaid, L.K. Vora, F. Volpe-Zanutto, A.H. Sabri, K. Peng, Q.K. Anjani, P. E. McKenna, A. Ripolin, E. Larrañeta, H.O. McCarthy, R.F. Donnelly, Microneedle array patches for sustained delivery of fluphenazine: a micron scale approach for the management of schizophrenia, Biomater Adv. 153 (2023), https://doi.org/10.1016/j.bioadv.2023.213526.

[29] E. Larrañeta, J. Moore, E.M. Vicente-Pérez, P. González-Vázquez, R. Lutton, A. D. Woolfson, R.F. Donnelly, A proposed model membrane and test method for microneedle insertion studies, Int. J. Pharm. 472 (2014) 65–73, https://doi.org/10.1016/j.ijpharm.2014.05.042.

[30] A.S. Cordeiro, I.A. Tekko, M.H. Jomaa, L. Vora, E. McAlister, F. Volpe-Zanutto, M. Nethery, P.T. Baine, N. Mitchell, D.W. McNeill, R.F. Donnelly, Two-photon polymerisation 3D printing of microneedle Array templates with versatile designs: application in the development of polymeric drug delivery systems, Pharm. Res. 37 (2020) 1–15, https://doi.org/10.1007/s11095-020-02887-9.

[31] I.K. Ramöller, M.T.A. Abbate, L.K. Vora, A.R.J. Hutton, K. Peng, F. Volpe-Zanutto, I.A. Tekko, K. Moffatt, A.J. Paredes, H.O. McCarthy, R.F. Donnelly, HPLC-MS method for simultaneous quantification of the antiretroviral agents rilpivirine and cabotegravir in rat plasma and tissues, J. Pharm. Biomed. Anal. 213 (2022) 114698, https://doi.org/10.1016/j.jpba.2022.114698.

[32] R.F. Donnelly, M.T.C. McCrudden, A.Z. Alkilani, E. Larrañeta, E. McAlister, A. J. Courtenay, M.C. Kearney, T.R. Raj Singh, H.O. McCarthy, V.L. Kett, E. Caffarel-Salvador, S. Al-Zahrani, A.D. Woolfson, Hydrogel-forming microneedles prepared from "super swelling" polymers combined with lyophilised wafers for transdermal drug delivery, PloS One 9 (2014), https://doi.org/10.1371/journal.pone.0111547.

[33] C.M. Berset, M.E. Caristo, F. Ferrara, P. Hardy, M. Oropeza-Moe, R. Waters, Federation of European Laboratory Animal Science Associations recommendations of best practices for the health management of ruminants and pigs used for scientific and educational purposes, Lab. Anim 55 (2021) 117–128, https://doi.org/10.1177/0023677220944461.

[34] E.M.A. Emea, Validation of Analytical Procedures: ICH Guidelines Q2, 2022. R2.

[35] J. Shao, J.C. Kraft, A. Clark, B. Li, J. Yu, J. Freeling, J. Koehn, R.J.Y. Ho, Nanodrug formulations to enhance HIV drug exposure in lymphoid tissues and cells: clinical significance and potential impact on treatment and eradication of HIV/AIDS, Nanomedicine (Lond) 11 (5) (2016) 545–564, https://doi.org/10.2217/nnm.16.1.

[36] Y. Nayak, K. Avadhani, S. Mutalik, U.Y. Nayak, Lymphatic delivery of anti-HIV drug nanoparticles, Recent Pat. Nanotechnol. 10 (2016) 116–127, https://doi.org/10.2174/1872210510999160414150818.

[37] A.J. Paredes, F. Volpe-Zanutto, L.K. Vora, I.A. Tekko, A.D. Permana, C.J. Picco, H. O. McCarthy, R.F. Donnelly, Systemic delivery of tenofovir alafenamide using dissolving and implantable microneedle patches, Mater. Today Bio. 13 (2022) 100217, https://doi.org/10.1016/j.mtbio.2022.100217.

[38] H.A. Ravin, A.M. Seligman, J. Fine, Polyvinyl pyrrolidone as a plasma expander — studies on its excretion, distribution and metabolism, N. Engl. J. Med. 247 (1952) 921–929, https://doi.org/10.1056/nejm195212112472403.

[39] T. Yamaoka, Y. Tabata, Y. Ikada, Comparison of body distribution of poly(vinyl alcohol) with other water-soluble polymers after intravenous administration, J. Pharm. Pharmacol. 47 (1995) 479–486, https://doi.org/10.1111/j.2042-7158.1995.tb05835.x.

[40] R.E.M. Lutton, E. Larrañeta, M.C. Kearney, P. Boyd, A.D. Woolfson, R.F. Donnelly, A novel scalable manufacturing process for the production of hydrogel-forming microneedle arrays, Int. J. Pharm. 494 (2015) 417–429.

[41] W. Li, R.N. Terry, J. Tang, M.R. Feng, S.P. Schwendeman, M.R. Prausnitz, Rapidly separable microneedle patch for the sustained release of a contraceptive, Nat. Biomed. Eng. 3 (2019) 220–229, https://doi.org/10.1038/s41551-018-0337-4.

[42] W. Li, J. Tang, R.N. Terry, S. Li, A. Brunie, R.L. Callahan, R.K. Noel, C. A. Rodríguez, S.P. Schwendeman, M.R. Prausnitz, Long-acting reversible contraception by effervescent microneedle patch, Sci. Adv. 5 (2019), https://doi.org/10.1126/sciadv.aaw8145.

[43] L.M. Kaminskas, C.J.H. Porter, Targeting the lymphatics using dendritic polymers (dendrimers), Adv. Drug Deliv. Rev. 63 (2011) 890–900, https://doi.org/10.1016/j.addr.2011.05.016.

[44] A.J. Paredes, A.D. Permana, F. Volpe-Zanutto, M.N. Amir, L.K. Vora, I.A. Tekko, N. Akhavein, A.D. Weber, E. Larrañeta, R.F. Donnelly, Ring inserts as a useful strategy to prepare tip-loaded microneedles for long-acting drug delivery with application in HIV pre-exposure prophylaxis, Mater. Des. 224 (2022) 111416, https://doi.org/10.1016/j.matdes.2022.111416.

[45] J.P. Freeling, J. Koehn, C. Shu, J. Sun, R.J.Y. Ho, Long-acting three-drug combination anti-HIV nanoparticles enhance drug exposure in primate plasma and cells within lymph nodes and blood, AIDS 28 (2014) 2627, https://doi.org/10.1097/QAD.0000000000000421.

[46] C. Qin, Y.J. Chu, W. Feng, C. Fromont, S. He, J. Ali, J.B. Lee, A. Zgair, M. Berton, S. Bettonte, R. Liu, L. Yang, T. Monmaturapoj, C. Medrano-Padial, A.A.R. Ugalde, D. Vetrugno, S.Y. Ee, C. Sheriston, Y. Wu, M.J. Stocks, P.M. Fischer, P. Gershkovich, Targeted delivery of lopinavir to HIV reservoirs in the mesenteric

lymphatic system by lipophilic ester prodrug approach, J. Control. Release 329 (2021) 1077–1089, https://doi.org/10.1016/J.JCONREL.2020.10.036.
[47] H.M. Patel, Serum opsonins and liposomes: their interaction and opsonophagocytosis, Crit Rev Ther Drug Carr. Syst. 9 (1992) 39–90. https://pubmed.ncbi.nlm.nih.gov/1544174/.
[48] W.J. Xu, J.X. Cai, Y.J. Li, J.Y. Wu, D. Xiang, Recent progress of macrophage vesicle-based drug delivery systems, drug Deliv, Transl. Res. 12 (2022) 2287–2302, https://doi.org/10.1007/s13346-021-01110-5.
[49] S.M. Stieger-Vanegas, P.M. Frank, Peritoneal space, in: Textb. Vet. Diagnostic Radiol., Seventh Ed, W.B. Saunders, 2018, pp. 764–791, https://doi.org/10.1016/B978-0-323-48247-9.00051-6.
[50] M. Núñez, Hepatotoxicity of antiretrovirals: incidence, mechanisms and management, J. Hepatol. 44 (2006) S132–S139, https://doi.org/10.1016/J.JHEP.2005.11.027.
[51] European mMedicines aAgency CHMP, Assessment report Edurant, international non-proprietary name: rilpivirine, procedure no. EMEA/H/C/002264, 2011.
[52] LiverTox, Rilpivirine - LiverTox - NCBI Bookshelf, 2017.
[53] R. Parasrampuria, S.L. Ford, Y. Lou, C. Fu, K.K. Bakshi, A.R. Tenorio, C. Trezza, W. R. Spreen, P. Patel, A phase I study to evaluate the pharmacokinetics and safety of cabotegravir in adults with severe renal impairment and healthy matched control participants, Clin. Pharmacol. Drug Dev. 8 (2019) 674–681, https://doi.org/10.1002/CPDD.664.
[54] S.R. Dyavar, S. Kumar, N. Gautam, A.T. Podany, L.C. Winchester, J.A. Weinhold, T. M. Mykris, P. Nallasamy, Y. Alnouti, C.V. Fletcher, Intramuscular and subcutaneous administration of antiretroviral drugs, compared with oral, enhances delivery to lymphoid tissues in BALB/c mice, J. Antimicrob. Chemother. (2021) dkab228, https://doi.org/10.1093/JAC/DKAB228.
[55] European Medicines Agency CHMP, Assessment report - Rekambys - Procedure No. EMEA/H/C/005060/0000, 2020.
[56] T.A. Kulkarni, A.N. Bade, B. Sillman, B.L.D. Shetty, M.S. Wojtkiewicz, N. Gautam, J.R. Hilaire, S. Sravanam, A. Szlachetka, B.G. Lamberty, B.M. Morsey, H.S. Fox, Y. Alnouti, J.E.M. McMillan, R.L. Mosley, J. Meza, P.L. Domanico, T.Y. Yue, G. Moore, B.J. Edagwa, H.E. Gendelman, A year-long extended release nanoformulated cabotegravir prodrug, Nat. Mater. 19 (2020) 910–920, https://doi.org/10.1038/s41563-020-0674-z.
[57] A.J. Paredes, I.K. Ramöller, P.E. McKenna, M.T.A. Abbate, F. Volpe-Zanutto, L. Vora, M. Kilbourne-Brook, C. Jarrahian, K. Moffatt, C. Zhang, I.A. Tekko, R. F. Donnelly, Microarray patches: breaking down the barriers to contraceptive care and HIV prevention for women across the globe, Adv. Drug Deliv. Rev. 173 (2021) 331–348, https://doi.org/10.1016/j.addr.2021.04.002.
[58] A. Ripolin, J. Quinn, E. Larrañeta, E.M. Vicente-Perez, J. Barry, R.F. Donnelly, Successful application of large microneedle patches by human volunteers, Int. J. Pharm. 521 (2017) 92–101, https://doi.org/10.1016/j.ijpharm.2017.02.011.
[59] R.K.R. Rajoli, C. Flexner, J. Chiong, A. Owen, R.F. Donnelly, E. Larrañeta, M. Siccardi, Modelling the intradermal delivery of microneedle array patches for long-acting antiretrovirals using PBPK, Eur. J. Pharm. Biopharm. 144 (2019) 101–109, https://doi.org/10.1016/J.EJPB.2019.09.011.